



Published in final edited form as:

J Med Chem. 2015 February 26; 58(4): 1846–1861. doi:10.1021/jm501680m.

Bis-Aryl Urea Derivatives as Potent and Selective LIM Kinase (Limk) Inhibitors

Yan Yin^{†,ϕ}, Ke Zheng[†], Nibal Eid^{‡,¥}, Shannon Howard^{‡,¥}, Ji-Hak Jeong[‡], Fei Yi[£], Jia Guo[£], Chul M Park^{§,†}, Mathieu Bibian[†], Weilin Wu[‡], Pamela Hernandez^{‡,¥}, HaJeung Park[∞], Yuntao Wu[£], Jun-Li Luo[‡], Philip V. LoGrasso^{‡,¥,*}, and Yangbo Feng^{*,†}

[†]Medicinal Chemistry, The Scripps Research Institute, Scripps Florida, 130 Scripps Way, #2A1, Jupiter, FL 33458

[‡]Discovery Biology, The Scripps Research Institute, Scripps Florida, 130 Scripps Way, #2A1, Jupiter, FL 33458

[∞]Crystallography/Modeling Facility, Translational Research Institute, Scripps Florida, 130 Scripps Way, #2A1, Jupiter, FL 33458

[¥]Department of Molecular Therapeutics, The Scripps Research Institute, Scripps Florida, 130 Scripps Way, #2A1, Jupiter, FL 33458

Department of Cancer Biology, The Scripps Research Institute, Scripps Florida, 130 Scripps Way, #2A1, Jupiter, FL 33458

^ϕSchool of Chemical and Environmental Engineering, Shanghai Institute of Technology, 100 Hai Quan Rd., Shanghai, 201418, P. R. China

[£]National Center for Biodefense and Infectious Diseases, School of System Biology, George Mason University, Manassas, VA 20110

Abstract

The discovery/optimization of *bis*-aryl ureas as Limk inhibitors to obtain high potency and selectivity, and appropriate pharmacokinetic properties through systematic SAR studies is reported. Docking studies supported the observed SAR. Optimized Limk inhibitors had high biochemical potency ($IC_{50} < 25$ nM), excellent selectivity against ROCK and JNK kinases (> 400-fold), potent inhibition of cofilin phosphorylation in A7r5, PC-3, and CEM-SS T cells ($IC_{50} < 1$ μ M), and good in vitro and in vivo pharmacokinetic properties. In the profiling against a panel of 61 kinases, compound **18b** at 1 μ M inhibited only Limk1 and STK16 with 80% inhibition. Compounds **18b** and **18f** were highly efficient in inhibiting cell-invasion/migration in PC-3 cells. In addition, compound **18w** was demonstrated to be effective on reducing intraocular pressure

Corresponding authors: Yangbo Feng: yfeng@scripps.edu, 561-228-2201; Philip V. LoGrasso: lograsso@scripps.edu, 561-228-2230.

§Present address: C.M.P. Korea Research Institute of Chemical Technology (KRICT), 141 Gajeongro, Yuseong, Korea 305–600.

Supporting information Available: Cofilin phosphorylation in PC-3 cells for compounds **18f** and **18h**, DMPK assay procedures, and detailed kinase profiling data for **18b** against a panel of 61 kinases. This material is available free of charge via the Internet at <http://pubs.acs.org>.

(IOP) on rat eyes. Taken together, these data demonstrated that we had developed a novel class of *bis*-aryl urea derived potent and selective Limk inhibitors.

Keywords

LIM kinase; Limk inhibitor; urea; cancer; glaucoma; cell invasion; infection

Introduction

LIM-kinase (Limk) is a serine-threonine protein kinase. Two isoforms were identified as LIM kinase 1 (Limk1) and LIM kinase 2 (Limk2).¹⁻⁴ Limk1 and Limk2 are highly homologous and share 50% overall identity. Both isoforms consist of two amino-terminal LIM domains, adjacent PDZ and proline/serine-rich regions, followed by a carboxyl-terminal protein kinase domain.⁵ Limk1 was found to be expressed widely in embryonic and adult tissues, with notably high expression in the brain, kidney, lung, stomach and testis.⁶ Limk2 was found to be expressed in almost all embryonic and adult tissues examined with the exceptions of glial cell, the testis, and kidney glomeruli.⁷ Upon activation by upstream signals, Limk phosphorylates its substrate cofilin at the Ser-3 residue, thereby inactivating it, and leading to dynamic regulation of actin cytoskeleton.⁸⁻¹² Accumulated evidences suggest that Limk activity is associated with a variety of diseases including Williams Syndrome,¹³ Alzheimer Disease (AD),^{14, 15} psoriatic epidermal lesions,¹⁶ primary pulmonary hypertension (PPH),^{17, 18} intracranial aneurysms (IA),¹⁹ ocular hypertension/glaucoma,²⁰ HIV and other viral infections,²¹⁻²⁴ and cancers and cancer cell migration/invasion.²⁵⁻³¹

Recent molecular biology studies reported that Limk1 was over-expressed in cancerous prostate cells and tissues,²⁶ reduced expression of Limk1 retarded PC3ASL cells' proliferation by arresting cells at G2/M phase,²⁶ altered expression of Limk1 changed cell morphology and organization of actin cytoskeleton in PC3 cells,²⁶ increased expression of Limk1 was associated with accumulation of chromosomal abnormalities and development of cell cycle defects in cells that naturally express lower concentrations of Limk1,²⁷ reduced expression of Limk1 abolished the invasive behavior of prostate cancer cells,²⁷ and expression of Limk1 is higher in prostate tumors with higher Gleason Scores and incidence of metastasis.²⁷ All these observations suggest the possibility of up-regulated Limk1 as a cellular oncogene, and inhibition of Limk1 activity in cancerous prostate cells and tissues could lead to reduction of phosphorylated cofilin and decrease of the cells' motility and thus the invasiveness of tumor cells and their evolution to metastasis. Therefore, small molecule inhibitors of Limk1 could be potential therapeutic agents for prostate cancers. Recent studies also suggest that use of Limk inhibitors may provide a novel way to target the invasive machinery in GBM (glioblastoma multiforme).³²⁻³⁴

HIV-1 binding and entry into host cells are strongly impaired by the inhibition of actin polymerization.^{24, 35} Wu *et al.* demonstrated that HIV-mediated Limk activation is through gp120-triggered transient activation of the Rac-PAK-Limk pathway, and that knockdown of Limk through siRNA decreased filamentous actin, increased CXCR4 trafficking, and diminished viral DNA synthesis.²³ Wen *et al.* showed that LIM kinases modulate retrovirus

particle release and cell-cell transmission events.²⁴ This research suggest that HIV hijacks Limk to control the cortical actin dynamics for the onset of viral infection of CD4 T cells. Therefore, Limk inhibitors are supposed to have high potentials as therapeutics in anti-HIV infection applications.²³

To the best of our knowledge, few small molecule Limk inhibitors have been reported in the literature.²⁸ Bristol-Myers Squibb pharmaceuticals (BMS) disclosed potent Limk1 inhibitors based on an aminothiazole scaffold.^{36, 37} Tel-Aviv University recently published an oxazole based Limk1/2 inhibitor (T56-Limki) from computer-aided drug design, which was found to be effective against cancer metastasis for treatment of neurofibromatosis.³⁴ A group of scientists from Australia reported 4-aminobenzothieno[3,2-d] pyrimidine based Limk1 inhibitors from high-through-put screen (HTS) showing activity in the micromolar range.^{38, 39} Recently, a Japanese group also reported a Limk inhibitor (Damnacanthol or Dam, natural product based) from HTS campaigns, and this compound (Dam) has a Limk1 inhibition IC_{50} of ~ 800 nM.³¹ Lexicon pharmaceuticals revealed a class of Limk inhibitors based on a piperidine urea or guanidine scaffold for the treatment of ocular hypertension and associated glaucoma.²⁰ More recently, the same group of Lexicon scientists reported a novel class of Type-III binding Limk2 inhibitors that are based on a sulfonamide scaffold.⁴⁰

Our group reported a novel pyrazole-phenyl urea scaffold **1** (Figure 1) as potent and selective Rho kinase (ROCK) inhibitors and their significant intraocular pressure (IOP) lowering effects on rat eyes.^{41, 42} Compound **1** had low Limk inhibition in counter-screen studies ($IC_{50} > 10 \mu M$). However, SAR investigation revealed that replacement of the hinge-binding moiety pyrazole in **1** with a 4-yl-pyrrolopyrimidine (compound **2**) significantly decreased its ROCK-II affinity (ROCK-II $IC_{50} = 188 \text{ nM}$ of **2** vs. 2 nM of **1**). On the other hand, compound **2** gained a modest Limk1 inhibition (Limk1 $IC_{50} = 642 \text{ nM}$ vs. $> 10 \mu M$ for **1**), revealing an interesting hinge-binder dependent kinase selectivity profile for this phenyl urea based scaffold. Further modification of compound **2** on its urea terminal side led to compound **3** (Figure 1) which had an even weaker ROCK-II affinity ($IC_{50} = 1365 \text{ nM}$) but improved Limk1 biochemical potency ($IC_{50} = 201 \text{ nM}$). Interestingly, the 4-yl-pyrrolopyrimidine moiety in **2** and **3** is also present in Lexicon's piperidine urea/guanidine based Limk inhibitors, and is believed to be involved in hinge-binding interactions.²⁰

Encouraged by the selectivity bias of compound **3** against Limk1 and ROCK-II, we carried out further optimization for this *bis*-aryl urea scaffold (starting from **3**), in the hope to discover highly potent, selective, and proprietary Limk inhibitors for various applications. Herein, we report the synthesis and structure-activity relationship (SAR) studies for this series of *bis*-aryl urea based Limk inhibitors.

Chemistry

Inhibitors **3** and **7** were accessed through a short route as shown in Scheme 1. Coupling 3-aminobenzoic acid with propan-2-amine gave carbonyl amide **4** in the presence of HATU as coupling reagent and DIEA as base. Mixing intermediate **4** with 1-bromo-4-isocyanatobenzene derivatives in dichloromethane (DCM) produced bromides **5**. Finally, targeted inhibitors **3** and **7** were synthesized through a Suzuki coupling with an appropriate

aryl boronic acid pinacol ester or alternatively *via* a two-step palladium catalyzed borylation/Suzuki coupling sequence with an aryl halide. Final targeted Limk inhibitors were all purified by the high pressure reverse-phase liquid chromatograph (HPLC) methodology to give a purity of 95% based on UV absorption (254 nm).

Pyrrolopyrimidines **10** were synthesized through the reaction of substituted anilines **8** with isocyanatobenzene derivatives in DCM at room temperature, followed by Pd-catalyzed borylation/Suzuki coupling reaction with 4-chloro-5-methyl-7*H*-pyrrolo[2,3-*d*]pyrimidine (Scheme 2).

The synthesis of *N*-substituted (on the urea NH attached to the central phenyl ring) compounds **14** is described in Scheme 3. To make **12b** and **12c** (**12a** is commercially available, where a methyl group is attached to the alinine), *N*-(4-bromophenyl)oxazolidin-2-one **11** was first prepared by reacting 4-bromo-aniline with 2-chloroethyl carbonochloridate in the presence of K₂CO₃ in CH₃CN. Intermediate **11** and a secondary amine pyrrolidine or piperidine were then dissolved in DMSO and heated at 110 °C for 1 h in a microwave reactor to give *N*-substituted 4-bromo-aniline **12b** (from pyrrolidine) and **12c** (from piperidine).⁴³ Mixing **12** and 1-isocyanato-4-methoxybenzene in DCM with stirring gave urea **13**. Finally, bromide **13** underwent a Pd-catalyzed borylation/Suzuki coupling reaction sequence to produce **14**.

The preparation of *N*-substituted (on the urea NH attached to the terminal phenyl ring) compound **18** is shown in Scheme 4. Addition of 2-chloroethyl carbonochloridate to a mixture of anilines and pyridine in DCM gave *N*-phenyl-oxazolidin-2-one derivative **15**.⁴⁴ Then, refluxing **15** and KOH in EtOH produced *N*-hydroxyethyl aniline **16**. Heating a mixture of iodobenzene, an *N,N'*-disubstituted ethanamine, Pd(dba)₂, BINAP, and Cs₂CO₃ in dioxane gave secondary aniline **17**.⁴⁵ Finally, inhibitors **18** were synthesized from **16** or **17** by following the synthetic procedures described in Scheme 3.

Results and discussion

Compounds prepared were first screened in biochemical assays against Limk1 (Reaction Biology Corporation, <http://www.reactionbiology.com>) and ROCK-II.^{46, 47} Selected potent Limk inhibitors were also counterscreened against ROCK-I, PKA,^{42, 46, 48} and JNK3,⁴⁹ as well as four selected P450 isoforms (1A1, 2C9, 2D6, and 3A4).^{46, 48, 50} Potent and selective Limk inhibitors were then evaluated in cell-based assays for their inhibition of cofilin phosphorylation in A7r5 cells. Due to the potential applications of Limk inhibitors for treatment of cancer and HIV-infection, selected lead inhibitors were also assessed in prostate carcinoma (PC-3) cell lines stimulated by hepatocyte growth factor (HGF),⁵¹ and in HIV related CEM-SS T cells²³ using Western blot analysis. To assess the drugability of these *bis*-aryl urea based Limk inhibitors, a few potent, selective, and membrane permeable compounds were further evaluated in *in vitro* and *in vivo* drug metabolism and pharmacokinetics (DMPK) studies.^{41, 46, 50, 52-55}

Since the variation of hinge-binding moieties could induce significant differences in kinase inhibition potency and selectivity, as indicated in Figure 1, we started SAR studies by

varying the heteroaryl ring of **3** in order to discover the best hinge binding moiety for this *bis*-aryl urea scaffold of Limk inhibitors. As shown in Table 1, compounds with a simple 5- or 6-membered heteroaromatic ring as the hinge-binding moiety, such as pyrazole, pyridine, and aminopyrimidine, are all basically ROCK inhibitors (**7a–7c**, $IC_{50} < 200$ nM) with low Limk1 inhibition ($IC_{50} > 10$ μ M). This observation was in accordance with our previous reports that pyrazole, pyridine, and aminopyrimidine were suitable hinge-binding moieties for developing ROCK inhibitors.^{41, 46, 50, 53, 54} Application of [5,6]-fused aromatic rings, such as pyrrolopyridine (**7d**) and purinone (**7e**) still yielded compounds with good ROCK-II inhibition ($IC_{50} = 132$ and 247 nM for **7d** and **7e**, respectively) but low Limk1 inhibition ($IC_{50} > 10$ μ M). However, the use of a 4-yl-purine moiety reversed the kinase selectivity between ROCK and Limk. Compound **7f** exhibited a slightly higher potency for Limk1 inhibition ($IC_{50} = 1.5$ μ M) than for ROCK-II inhibition ($IC_{50} = 5.6$ μ M). Interestingly, changing hinge-binding group from the purine in **7f** to a pyrrolopyrimidine ring in **3** significantly enhanced the Limk1 inhibition potency and the selectivity against ROCK. Moreover, substitution of a methyl group on the 5-position of the pyrrolopyrimidine ring (**7g**) further improved the inhibition potency over Limk1 ($IC_{50} = 62$ nM vs. 201 nM for **3**) and the selectivity against ROCK-II ($IC_{50} = 1608$ nM). Interestingly, application of 6-methyl pyrrolopyrimidine and 5,6-dimethyl pyrrolopyrimidine rings (**7h** and **7i**) gave slightly lower Limk1 inhibition ($IC_{50} = 80$ nM) but better selectivity over ROCK-II. Therefore, further optimizations for other parts of **3** will use 5-methyl pyrrolopyrimidine as the hinge-binding moiety. However, the 5,6-dimethyl pyrrolopyrimidine moiety will also be used in preparing drug candidate Limk inhibitors since it could lead to higher selectivity and better DMPK properties (Tables 5&6&7).

For the convenience of compound synthesis, SAR studies for the central phenyl ring were mainly based on substitutions at its *ortho*-position (to the urea moiety). As shown in Table 2, three substitutions were evaluated. Compared to the non-substituted inhibitor **7g**, the trifluoromethyl substitution yielded a compound (**7j**) that had a similar Limk1 inhibition potency ($IC_{50} = 60$ nM vs. 62 nM for **7g**) but lower selectivity (ROCK-II $IC_{50} = 976$ nM vs. 1608 nM for **7g**). However, substitution by a small F group (with a size close to that of a proton, compound **7k**) led to both enhanced Limk1 inhibition ($IC_{50} = 18$ nM) and improved selectivity against ROCK-II (based on IC_{50} values, the selectivity over ROCK-II is 26-fold and 43-fold for **7g** and **7k**, respectively, Table 2). On the other hand, substitution by a large dimethylaminoethoxy side chain (**7l**) significantly decreased both the Limk1 inhibition ($IC_{50} = 710$ nM vs. 62 nM for **7g**) and the selectivity over ROCK-II (Table 2). Therefore, an *ortho*-F-substitution on the central phenyl ring is the best choice for preparing a highly potent and selective Limk inhibitor.

SAR was next investigated on the terminal phenyl ring of compound **7g**, where a 5-methylpyrrolopyrimidine is used as the hinge-binding moiety and the central phenyl group is non-substituted for the convenience of organic synthesis. As shown in Table 3, removal of the 3-carbonyl amide from the terminal phenyl ring of **7g** yielded a compound (**10a**) with a lower Limk1 inhibitory activity ($IC_{50} = 142$ nM for **10a** vs. 62 nM for **7g**). Interestingly, replacing the 3-carboxyl amide with a F group (**10b**) significantly reduced the Limk1 inhibition ($IC_{50} = 315$ nM), which is probably due to special F-bonding interactions⁵⁶

between this F group and its surrounding protein residues under the p-Loop (see Figure 3 of docking studies). This special F-bonding interaction might disturb the optimal binding conformation of these urea based Limk inhibitors. The same effects were also observed in several other Limk inhibitors (see Table 4). It is important to point out that this special effect of F-bonding interactions was not observed for F-substitutions on the central phenyl ring (**7k**, Table 2), indicating that this effect is dependent on the position of F-substitutions. Actually, we have observed similar negative effects (reducing kinase inhibition potency) of F-bonding interactions in developing our ROCK-II inhibitors⁵³ and JNK3 inhibitors,⁵⁵ where the F-substituted aromatic moieties are all bound to an area under the p-Loop inside the ATP-binding pocket of proteins kinases.

Unlike F-substitutions, replacing the 3-carboxyl amide with a methoxy group resulted in a Limk inhibitor (**10d**) that had a similar Limk1 inhibitory potency ($IC_{50} = 75$ nM vs. 62 nM for **7g**) and a slightly better selectivity over ROCK-II (Table 3). However, the 2-methoxy substitution (**10c**) significantly reduced the Limk1 inhibition activity ($IC_{50} = 283$ nM). On the other hand, the 4-methoxy substitution (**10e**) enhanced both Limk1 inhibition ($IC_{50} = 35$ nM) and selectivity against ROCK-II ($IC_{50} > 10$ μ M, selectivity > 285-fold). Similar SAR patterns were also obtained for F-, Cl-, and methyl-substitutions on this terminal phenyl group (see Table 4), indicating that 4-substitution is the best fit for this scaffold in Limk inhibitions. Heteroaryl rings other than the benzene ring were also evaluated as the terminal aromatic moieties. For example, application of a 2-yl-thiazole (**10f**) resulted in lower Limk1 inhibition (compared to **10a**); and the use of a 2-yl-pyridine moiety (**10g**) almost inactivated the compound against both Limk1 and ROCK-II.

Investigation of the substitution effects on the two urea NH groups was the next focus in our SAR studies. For the urea NH attached to the central phenyl ring, neither small nor large substitutions including pyrrolidinoethyl and piperidinoethyl could be tolerated. As shown in Figure 2, a simple methyl substitution (**14a**) would significantly reduce the Limk1 inhibitory potency ($IC_{50} = 1090$ nM vs. 35 nM for **10e**). Larger substitutions to this NH group gave even lower Limk1 inhibitions, as evidenced by the Limk1 IC_{50} values of compounds **14b** and **14c** (Figure 2). These results demonstrated that alkylation to this urea NH disturbed the optimal binding conformations, or the NH is involved in H-bonding interactions to the protein, thus resulted in a low Limk affinity (also see docking modes in Figure 3).

In contrast to observations in Figure 2, SAR studies demonstrated that substitutions on the urea NH group attached at the terminal phenyl ring were well tolerated, and excellent Limk inhibitors could be obtained through this modification. As shown in Table 4, a pyrrolidinoethyl substitution yielded a compound (**18a**) with slightly lower Limk1 inhibition ($IC_{50} = 368$ nM vs. 142 nM for **10a**). However, replacing the pyrrolidine ring with a hydroxyl group (**18b**) led to both a high Limk1 inhibitory activity ($IC_{50} = 43$ nM vs. 142 nM for **10a**) and a good selectivity over ROCK-II ($IC_{50} = 6565$ nM vs. 2358 nM for **10a**). Inspired by **18b**, a small library of $4 \times 3 = 12$ analogs (of **18b**), based on four functional groups (F-, Cl-, Methyl, and Methoxy) and three substitution patterns on the terminal phenyl ring (2-, 3-, 4-positions), were prepared and evaluated (compounds **18c** to **18n**, Table 4). Generally, the 4-substitution exhibited the highest and the 2-substitution gave the lowest Limk1 inhibitory activity. Selectivity against ROCK-II followed the same pattern with the 4-

substitution being the highest and 2-substitution the lowest, no matter what was the substitution group. Among the 4-substituted Limk inhibitors, the 4-Cl analog had the best Limk1 inhibitory potency (**18h**, $IC_{50} = 25$ nM) and its 4-F counterpart (**18e**, $IC_{50} = 86$ nM) had the lowest Limk affinity probably due to the special F-bonding interactions,⁵⁶ while the Limk1 inhibitory activity and the selectivity against ROCK-II for the methyl and methoxy analogs (**18k** and **18n**) were in between.

To confirm that alkylation to this urea NH group could be well tolerated, two more substitutions were explored. As shown in Table 4, aminoethyl and *N,N'*-dimethylaminoethyl substitutions were applied to both 4-Cl- and 4-methoxyphenyl ureas, and the resulting 4 compounds **18o** to **18r** all exhibited high Limk1 inhibitions. Compounds **18p** to **18r** were assessed in counter-screen studies, and **18q** and **18r** were found to have high selectivity against ROCK-II ($IC_{50} > 10$ μ M, selectivity is > 210 -fold and > 500 -fold for **18q** and **18r**, respectively) while that for **18p** was only ~ 21 -fold. The lower Limk1 inhibition potency observed for **18a**, as compared to **18q** and **18r**, might be due to its bulky pyrrolidine ring which might have disturbed the optimal binding conformation.

Computer modeling studies of lead compounds demonstrated that these *bis*-aryl urea based Limk inhibitors are all Type-I ATP-competitive kinase inhibitors. The docking mode of compound **18b** in the crystal structure of Limk1 protein (PDB ID 3S95) is shown in Figure 3. Key interactions in this motif include: two H-bonds between the pyrrolopyrimidine N/NH (N1 and N7) and hinge residue I416; one plausible H-bond between N3 of pyrrolopyrimidine ring and the side chain OH group of residue T413 (not labeled in Figure 3 since this H-bonding requires rotation movement of the T413 side chain); one H-bond between the urea carbonyl moiety and the side chain amino group of K368; one H-bond between the OH group and residue D478; cation- π interactions between the terminal phenyl ring and the side chain amino group of K368; hydrophobic interactions between the terminal phenyl ring and its surrounding residues under the P-loop. It is important to point out that hydrophobic interaction between the aromatic rings of pyrrolopyrimidine/central phenyl moieties and their surrounding side chains of protein residues also contributed to the high affinity of these Limk inhibitors.

The binding motif of compound **18b** supported our observed SAR. For example, both mono- and *bis*-methyl substituted (to the 5- and/or 6-position), or even larger group substituted (unpublished results) pyrrolopyrimidine rings were well tolerated due to the open space around this area, and these substitutions could enhance the inhibitor's Limk inhibition due to the extra interactions introduced by substitution(s). Substitution to the urea NH attached to the central phenyl ring led to inactive compounds because this substitution could disturb the orientation of the urea carbonyl group thus weakening its H-bonding to K368. On the other hand, substitutions to the urea NH adjacent to the terminal phenyl ring were well tolerated and could lead to enhanced Limk inhibition since there is enough space around this area and the substitution is directed toward the solvent. 4-Substitutions on the terminal phenyl group gave the most active Limk inhibitors (compared to the 2- and 3-substitutions) because there is a deep hydrophobic pocket around there. The H-bonding interaction between the pyrrolopyrimidine N3 and the side chain OH of T413 explained why compound **3** (Table 1) was a good Limk inhibitor while compound **7d** had low Limk1 inhibition. The significant

decrease of Limk1 inhibition in **7f** as compared to **3** (Table 1) is probably due to the extra H-bonding interactions between N5 (of **7f**) and surrounding protein residues, which might disturb the optimal binding conformation of the ligand thus reduce its affinity toward Limk1.

To summarize, our SAR analysis and docking studies for this *bis*-aryl urea based scaffold of Limk inhibitors showed that both 5- and 6-methyl-4-yl-pyrimidines, and the 5,6-dimethyl-4-yl-pyrrolopyrimidine could serve well as hinge-binding moieties for Limk inhibition. Among them, the 5,6-dimethylpyrrolopyrimidine was the best considering that it could render much better selectivity (against ROCK) and higher microsomal stability (see Table 6). An *ortho*-F-substitution on the central phenyl ring (to the urea moiety) could improve the Limk inhibitory potency while still keeping high microsomal stability (Table 6). On the other hand, an F-substitution on the terminal phenyl ring reduced inhibitory potency against Limk1 probably due to the special F-bonding interactions (under the P-loop). SAR analysis also indicated that a 4-Cl or a 4-methyl substitution on the terminal phenyl group gave overall best Limk inhibitors. Remarkably, a substitution to the urea NH attached on the terminal phenyl side could improve both biochemical and cell potency, enhance selectivity, and more importantly, increase the inhibitor's DMPK properties and bioavailability (see Table 7 below).

To take advantage of the important SAR information above, Limk inhibitors that combine the best structural elements from SAR analysis were thus prepared and evaluated. Table 5 lists the structures and biochemical potency data for four representative compounds. In compounds **18s** to **18w**, a 4-yl-5,6-dimethylpyrrolopyrimidine was used as the hinge binding moiety for optimal microsomal stability and better selectivity; An *ortho*-F-substitution on the central phenyl ring and a 4-Cl substitution on the terminal phenyl group were employed in order to achieve higher Limk1 potency; Representative substitutions on the terminal urea NH were applied to further investigate the DMPK properties (see discussion for Tables 6&7). Indeed, these compounds all had excellent Limk1 potency ($IC_{50} \approx 21$ nM) and good selectivity against ROCK-II ($IC_{50} > 20$ μ M for **18w** and **18x**).

In order to examine the selectivity profile of these *bis*-aryl urea based Limk1 inhibitors, selected lead compounds were subjected to counter screening against ROCK-I, JNK3 and four representative cytochrome P450 isoforms. As summarized in Table 6, these Limk inhibitors all exhibited low inhibitory activity over tested kinases and P450 enzymes, except that **7i** showed modest inhibition against enzyme 1A2 (77%) at 10 μ M. In addition to counterscreens against ROCK and JNK3, lead inhibitor **18b** was also profiled against a panel of 61 kinases (Reaction Biology Corporation, <http://www.reactionbiology.com/webapps/site/>). Results showed that **18b** at 1.0 μ M inhibited only Limk1 and STK16 with 80% inhibition (~ 3% hit ratio), and hit also Aurora-a, Flt3, LRRK2, and RET with >50% inhibition (~ 10% hit ratio). Detailed profiling data for **18b** is provided in Supporting Information. The profiling data demonstrated that selective Limk inhibitors can be obtained from this *bis*-aryl urea based scaffold.

These Limk inhibitors also had good to excellent stability in human and rat liver microsomes (Table 6) with good to excellent half-lives. It is important to point out that,

compared to the mono-methyl substituted pyrrolopyrimidine based analog **7g**, the 5,6-dimethyl pyrrolopyrimidine based Limk inhibitors **7i**, **18s**, and **18t** exhibited a higher stability in both human and rat microsomes, and a higher selectivity against ROCK (see also Tables 2&5). However, when the hydroxyl or the amino group on **18s** and **18t** was methylated, as shown in **18w** and **18x**, there was a significant drop in the microsomal stability (Table 6). Apparently, the lower stability of **18w** and **18x** was mainly due to demethylation on their side chain dimethylamino or methoxy groups. Other important SAR information from the selectivity profiling and stability data in Table 6 include, 1) all hydroxyethyl substituted (to the urea NH) compounds (**18 series**) had excellent stability in human liver microsomes with the exception of **18g** ($t_{1/2} = 22$ min only), 2) F-substitution on the central phenyl ring did not reduce the microsomal stability while still keeping the excellent selectivity (**7k** vs. **7g**), 3) F-substitution on the terminal phenyl ring not only reduced the Limk1 inhibitory potency (compared to its Cl-, methyl, and methoxy substituted counterparts) but also deteriorated the microsomal stability (**18e** vs. **18b**, **18h**, **18k**, and **18n**), 4) 3-substitution on the terminal phenyl ring led to significant reduction of microsomal stability, as compared to its 4-substituted counterpart (**18g** vs. **18h** and **18m** vs. **18n**), to the non-substituted analog (**18b**), and even to its 2-substituted analog (**18f**).

In an effort to investigate the cell-based activity of these Limk1 inhibitors, we monitored the phosphorylation state of cofilin in several cell lines. Data in A7r5 cells (Table 6) showed that inhibitors without any substitutions on their urea NH group (**7g**, **7i**, **7k**) had a cell activity of IC_{50} values only in the micromolar range. On the other hand, Limk inhibitors with their urea NH group (the one attached to the terminal aryl ring) substituted by a hydroxyethyl, or an aminoethyl, or a methoxyethyl, or a dimethylaminomethyl group (**18b** to **18x**) had IC_{50} values all in the sub-micromolar range, with the best one close to 100 nM (**18h**). In addition, SAR patterns shown in the cell-based potency were similar to those observed in biochemical potency and selectivity assays. For example, 4-Cl (**18h**) and 4-methyl (**18k**) substitutions produced compounds with better cell activity than 4-methoxy (**18n**) substitutions, and the 4-substitution exhibited the highest cell activity among 2-, 3-, and 4-substitutions (**18f**, **18g**, and **18h**) on the terminal phenyl ring.

Since Limk inhibitors could find wide applications, such as in glaucoma,²⁰ cancer,^{27, 28, 57, 58} infection,^{21-24, 59} and Alzheimer's disease (AD)^{14, 15} etc., cofilin phosphorylation assays were also carried out for a few selected lead compounds in prostate carcinoma (PC3) cell lines stimulated by hepatocyte growth factor (HGF) and in HIV-related CEM-SS T cell lines.⁶⁰ As shown in Figure 4, inhibitor **18b** exhibited significant inhibition even at a concentration of only 50 nM in Western blot analysis of cofilin phosphorylation in PC-3 cells (Figure 4A). Similar cell-based potency was also observed for **18f** and **18h** in PC-3 cells (see Supporting Information). The phosphorylation status of p-cofilin in CEM-SS T cells for inhibitors **18p**, **18r**, and **18x** is shown in Figure 4B. Again > 50% inhibition was seen for all these compounds at 1 μ M, an inhibitory potency similar to that obtained in A7r5 cells. The results from these three tested cell lines demonstrated that the optimized Limk inhibitors had good cell permeation. Compounds **18p** and **18r** had almost the same biochemical Limk1 potency (IC_{50} values were both ~ 20 nM, Table 4). Apparently, the better cell potency observed for **18r** than for **18p** (Figure 4B) is due to the

free NH₂ group present in **18p**, a structural element normally associated with deteriorated cell penetration.

In vivo pharmacokinetics (PK) studies were conducted for selected compounds during the whole optimization at various stages in order to identify structural elements that are favorable for in vivo applications, and/or to evaluate the feasibility of optimized Limk inhibitors for animal studies. PK properties of iv dosing (1 mg/kg) and the oral bioavailability (%F) for selected lead Limk inhibitors are listed in Table 7. Generally, a 2-hydroxyethyl side chain reduced the clearance (Cl) compared to the non-substituted (NH) urea derivatives (**10a**, **18b**, **18h**, **18k**, **18n** vs. **7g** and **7k**). In contrast, a side chain containing a terminal amino group increased the clearance significantly (**18o**, **18p**, **18r** vs. **18h**, **18k**, and **18n**). Remarkably, the high clearance of compounds with an amino side chain could be reduced dramatically by introducing an F-substitution on the central phenyl ring, or by using a 5,6-dimethylpyrrolopyrimidine (instead of the 5-methylpyrrolopyrimidine) as the hinge-binding moiety, or a combination of both (**18w** vs. **18r**). All Limk1 inhibitors listed in Table 7 had reasonable volume of distribution (Vd) values except a few which possessed an amino side chain and in which a 5-methylpyrrolopyrimidine was used as the hinge binding moiety (**18o**, **18p**, and **18r**). The much lower Cl and Vd values and higher AUC value for **18w** as compared to those for **18r** (and also for **18o** and **18p**) further demonstrated that an F-substitution on the central phenyl ring and the application of a 5,6-dimethylpyrrolopyrimidine as the hinge-binding moiety can improve the inhibitor's PK properties.

The PK data in Table 7 showed that substitution to the urea NH group could generally increase the half-lives of these urea based Limk inhibitors (the **10** and **18** series vs. the **7** series). The AUC and Cmax properties for these compounds were also excellent except for the three inhibitors (**18o**, **18p**, and **18r**) which contained an amino side chain and no F-substitutions on their central phenyl ring and in which a 5-methyl pyrrolopyrimidine was used as the hinge-binding moiety. It is important to point out that, even with an amino side chain, inhibitor **18w** still exhibited good AUC and Cmax values, probably due to the presence of both an F-substitution on the central phenyl ring and a 5,6-dimethylpyrrolopyrimidine moiety in its structure. Data in Table 7 also indicated that, while the non-substituted urea compounds (**7g** and **7k**) had no oral bioavailability (%F) at all, all inhibitors containing a hydroxyethyl side chain could exhibit reasonable oral bioavailability. However, those inhibitors containing an amino side chain (**18o**, **18p**, and **18r**) had no oral bioavailability either, probably because of the high clearance (Cl) exhibited by these compounds.

Since Limk1 expression is highly expressed in cancerous prostate cells and predominantly found in metastatic prostate tumor tissues, and is required for cancer cell migration and invasion,^{61, 62} Limk1 is considered as a biomarker for prostate cancer progression.⁶³ Limk1 is involved in Rac-induced actin cytoskeleton reorganization through inactivating phosphorylation of cofilin, and also mediated with focal adhesion complexes.^{8, 64} Reorganization of cytoskeleton is an essential feature of motility, detachment, and invasion of cancer cells. Moreover, Limk1 expression is correlated with the aggressiveness of cancer cells, and Limk1 expression in metastatic PC-3 cells is higher than less-aggressive LNCaP

and M21 cells.²⁶ To confirm the role of Limk inhibitors on the invasion and migration of prostate cancers, we examined the effect of optimized Limk inhibitors in PC-3 cells using an in vitro invasion assay or in vitro migration assay. Thus, Transwell chambers were coated with GFR Matrigel, and PC-3 cells were seeded in the insert of the chamber as described in the Experimental Section. After incubating for 48 hours, the invasive PC-3 cells were counted and analyzed by hematoxylin staining under microscope. As shown in Figure 5 for two representative inhibitors **18b** or **18f**, the invasion of PC-3 cells was significantly inhibited by the treatment of 1 μ M Limk inhibitors (76% for **18b**, and 83% for **18f**, compared to the control).

To verify the role of Limk inhibitors on migration of PC-3 cells, a wound was created by scratching in a cell monolayer as described in the Experimental Section. After incubating for 24 hours with treatment of inhibitors **18b** or **18f**, the closed wound area, indicating migrated cells, was analyzed by ImageJ software (Ver 1.48). As shown in Figure 6, the migrated PC-3 cells were decreased significantly even at a concentration as low as 0.1 μ M, and the migration was inhibited 74% by 1 μ M of inhibitor **18b** (16.5% (NS) by 0.1 μ M, 74.0% ($p < 0.01$) by 1 μ M, and 77.5% ($p < 0.01$) by 10 μ M compared to the control). Similar inhibition potency was also obtained for inhibitor **18f** (13.0% (NS) by 0.1 μ M, 76.1% ($p < 0.01$) by 1 μ M, and 81.0% ($p < 0.01$) by 10 μ M, compared to the control). These results indicated that **18b** or **18f** had inhibitory effects on invasion and migration of metastatic PC-3 cells. Considering that both inhibitors had low inhibition against ROCK-I and ROCK-II (Tables 4&6), the inhibition of which could also lead to suppression of cell migration/invasion,^{65, 66} results in Figures 5&6 also demonstrated that **18b** and **18f** must have played a role in Limk inhibitions in vitro.

To demonstrate the potential application of these Limk inhibitors for the treatment of glaucoma, the intraocular pressure (IOP)-lowering effect of compound **18w** was monitored after applying it topically on rat eyes (Brown Norway rats, $n = 6$ /group, housed under constant low-light conditions)⁶⁷ followed a protocol described previously by our groups.^{41, 53} Thus, compound **18w** was applied to the right eyes of an elevated IOP rat model (initial IOP was ~ 28 mmHg) using a dose of 50 μ g (20 μ L drop of a 0.25% solution). As shown in Figure 7, significant decreases in IOP were detected at 4 h, slightly weakened at 7 h, and IOP returning to baseline at 24 h as compared to the vehicle. It must be pointed out that the IOP drop could not be due to ROCK inhibition since **18w** had a high selectivity against ROCK (Table 5).

Conclusion

Through the application of a 4-yl-pyrrolopyrimidine as the hinge-binding moiety to replace the pyrazole group in ROCK inhibitor **1**, we identified compounds with high Limk1 inhibition potency. Systematic SAR studies around this *bis-aryl* urea scaffold (**3**) have led to a series of potent and selective Limk inhibitors. Docking studies demonstrated that these *bis-aryl* urea Limk inhibitors exhibited a typical Type-I kinase binding motif. The optimized Limk inhibitors had high biochemical potency and high selectivity over ROCK-I, ROCK-II, and JNK3. Inhibitor **18b** (also coded as SR-7826) was found to hit only Limk1 and STK16 with 80% inhibition at 1 μ M against a panel of 61 kinases. The lead Limk inhibitors also

had good cell-based potency in cofilin phosphorylation assays and in cell-based migration/invasion assays. In addition, they had fair to excellent in vitro and in vivo DMPK properties, such as a clean inhibition profile against select CYP-450 isoforms, a high stability in human and rat liver microsomes, and favorable PK properties in iv dosing (high AUC/Cmax, low *Cl*, and long half-lives) and fair to good oral bioavailability (**18b**, **18k**, **18n**, and **18s**) in rats. For example, compounds **18s** to **18x** (also coded as SR-11157) all had excellent potency against Limk1 (IC₅₀s = 21 nM), good cell-based activity against cofilin phosphorylation in A7r5 cells (IC₅₀s = 320 nM), and high selectivity over ROCK and JNK. The optimized inhibitors, such as **18b** and **18f**, showed excellent activities in migration/invasion cell-based assays. In addition, significant IOP drop on rat eyes (> 20%) was achieved for inhibitor **18w** (also coded as SR-11124) after topical administration (at a dose of 50 µg). Applications of optimized Limk inhibitors on other indications are under investigation and will be reported in due course.

Experimental Section

Commercially available reagents and anhydrous solvents were used without further purification unless otherwise specified. Thin layer chromatography (TLC) analyses were performed with precolated silica gel 60 F254. The mass spectra were recorded by LC/MS with Finnigan LCQ Advantage MAX spectrometer of Thermo Electron®. Flash chromatography was performed on prepacked columns of silica gel (230–400 Mesh, 40–63 µm) by CombiFlash® with EtOAc/hexane or MeOH/DCM as eluent. The preparative HPLC was performed on SunFire C₁₈ OBD 10µm (30 × 250 mm) with CH₃CN + 50% MeOH / H₂O + 0.1% TFA as eluent to purify the targeted compounds. Analytic HPLC was performed on Agilent technologies 1200 series with CH₃CN (Solvent B) / H₂O + 0.9% CH₃CN + 0.1% TFA (Solvent A) as eluent and the targeted products were detected by UV in the detection range of 215–310 nm. All compounds were determined to be > 95% pure by this method. NMR spectra were recorded with a Bruker® 400 MHz spectrometer at ambient temperature with the residual solvent peaks as internal standards. The line positions of multiplets were given in ppm (δ) and the coupling constants (*J*) were given in Hertz. The high-resolution mass spectra (HRMS, electrospray ionization) experiments were performed with Thermo Finnigan orbitrap mass analyzer. Data were acquired in the positive ion mode at resolving power of 100000 at *m/z* 400. Calibration was performed with an external calibration mixture immediately prior to analysis.

General synthetic procedures

The mixture of 3-aminobenzoic acid (10 mmol), propan-2-amine (10 mmol), HATU (10 mmol), and DIEA (30 mmol) in DMF (10 mL) was stirred at room temperature until the complete conversion of the started material. Then, saturated NaHCO₃ was added to quench the reaction and extracted with ethyl acetate (3 × 15 mL). The organic layers were combined, dried over anhydrous Na₂SO₄ and concentrated *in vacuo* to give crude aniline carboxamide **4**. Aniline **4** (0.2 mmol) was then added to the solution of isocyanatobenzene derivatives (0.2 mmol) in DCM (1 mL). The mixture was stirred at room temperature for 2 h. Then, the solvent was removed *in vacuo* to give the crude bromide **5** for next step without further purification.

The mixture of substituted anilines **8** (0.2 mmol) and isocyanatobenzene derivatives (0.2 mmol) in DCM (1 mL) was stirred at room temperature for 2 h, then the solvent was removed *in vacuo* to give the crude bromides **9** for next step without further purification.

2-Chloroethyl carbonochloridate (10 mmol) was added to a mixture of 4-bromo-aniline (10 mmol) and K₂CO₃ (30 mmol) in CH₃CN (100 mL) and the reaction was stirred for 24 h. Then, solvent was removed *in vacuo* and the remaining residue redissolved in water and ethyl acetate. The organic layers were combined, dried over anhydrous Na₂SO₄, concentrated *in vacuo*, and purified through silica gel to give crude *N*-(4-bromophenyl)oxazolidin-2-one **11**. Then **11** (0.2 mmol) and secondary amine (0.6 mmol) including pyrrolidine and piperidine were dissolved in DMSO (1 mL) and heated at 110 °C in microwave. After the complete conversion of **11**, the mixture was diluted with water and extracted with ethyl acetate. The organic layers were combined, dried over anhydrous Na₂SO₄ and concentrated under reduced pressure to give the intermediates **12a–12c**. The mixture of **12a–12c** (0.2 mmol) and 1-isocyanato-4-methoxybenzene (0.2 mmol) in DCM (1 mL) was stirred at room temperature for 2 h, the solvent was then removed *in vacuo* to give the crude bromide **13a–13c** for next step without further purification.

Finally, the boronic acid pinacol ester (0.3 mmol) and the crude bromide **5** (0.2 mmol) were dissolved in degassed 5:1 dioxane/H₂O. Pd(PPh₃)₄ (0.02 mmol) and 2M solution of K₂CO₃ (0.6 mmol) were added sequentially under Argon and the mixture was heated at 95 °C for 2 h. After cooling to room temperature, the mixture was diluted with water and extracted with ethyl acetate (3 × 5 mL). The organic layers were combined, dried over anhydrous Na₂SO₄ and concentrated *in vacuo*. The residue was then purified by preparative HPLC to give the targeted product **7a** and **7b** as white solid.

In an alternative route, *bis*-(pinacolato)diboron (0.24 mmol), crude **5**, **9**, and **13** (0.2 mmol), and PdCl₂(dppf) (0.02 mmol) were dissolved in degassed dioxane (5 mL). After refluxing for 2 h, the mixture was diluted with water and extracted with ethyl acetate (3 × 5 mL). The organic layers were combined, dried over anhydrous Na₂SO₄ and concentrated *in vacuo* to give crude boronic acid pinacol ester. Followed the synthesis procedure of **7a**, **7c–7k**, **10a–10f**, **14a–14c** were synthesized from crude boronic acid pinacol ester (0.2 mmol) and Ar-Cl (0.2 mmol).

2-Chloroethyl carbonochloridate (1 mmol) was added to a mixture of substituted anilines (1 mmol) and pyridine (3 mmol) in DCM (10 mL) and the reaction was stirred for 24 h. Then, solvent was removed *in vacuo* and the remaining residue redissolved in water and ethyl acetate. The organic layers were combined, dried over anhydrous Na₂SO₄ and concentrated *in vacuo* to give crude **15**. KOH (10 mmol) was added to the mixture of crude **15** (1 mmol) in EtOH (10 mL). Then the mixture was refluxed until the complete conversion of **15**. The solvent was removed *in vacuo* and the remaining residue was redissolved in water and ethyl acetate. The organic layers were combined, dried over anhydrous Na₂SO₄, concentrated *in vacuo*, and purified by silica gel to give intermediates **16**. The mixture of iodobenzene (0.2 mmol), 2-(pyrrolidin-1-yl)ethanamine (0.6 mmol), Pd(dba)₂ (0.01 mmol), BINAP (0.01 mmol), and Cs₂CO₃ (0.6 mmol) in dioxane (1 mL) was refluxing for 24 h. After cooling to room temperature, water and ethyl acetate were added. Then the organic layers were

combined, dried over anhydrous Na₂SO₄, concentrated *in vacuo*, and purified by silica gel to give intermediates **17**. Then **18a** and **18b–18n** were synthesized from **17** and **16** respectively followed the synthetic procedure of **10a–10f** from **8**.

3-(3-(4-(7*H*-pyrrolo[2,3-*d*]pyrimidin-4-yl)phenyl)ureido)-*N*-isopropylbenzamide (3)—45% yield in 4 steps. ¹H-NMR (DMSO-*d*₆, 400 MHz) δ 12.28 (s, br, 1H), 9.06 (s, 1H), 8.96 (s, 1H), 8.81 (s, 1H), 8.18–8.16 (m, 3H), 7.87 (s, 1H), 7.71–7.64 (m, 4H), 7.46–7.44 (m, 1H), 7.38–7.36 (m, 1H), 6.95 (s, 1H), 4.14–4.07 (m, 1H), 1.18 (d, *J* = 5.2 Hz, 6H); ¹³C-NMR (DMSO-*d*₆, 100 MHz) δ 165.50, 152.70, 152.38, 152.19, 147.81, 143.00, 139.47, 135.77, 130.01, 129.56, 128.51, 127.01, 120.81, 120.71, 118.10, 117.70, 113.78, 101.66, 40.95, 22.27; LC/MS (M+H⁺): 415.11; HRMS (ESI-Orbitrap) Calcd for C₂₃H₂₃N₆O₂: 415.1882 [M+H⁺], Found 415.1872.

3-(3-(4-(1*H*-pyrazol-4-yl)phenyl)ureido)-*N*-isopropylbenzamide (7a)—68% yield in 3 steps. ¹H-NMR (DMSO-*d*₆, 400 MHz) δ 12.86 (s, br, 1H), 8.82 (s, 1H), 8.69 (s, 1H), 8.18–8.16 (m, 1H), 7.96–7.93 (m, 1H), 7.84–7.79 (m, 1H), 7.78–7.74 (m, 1H), 7.72–7.68 (m, 1H), 7.65–7.60 (m, 1H), 7.53–7.51 (m, 2H), 7.45–7.41 (m, 3H), 7.36–7.32 (m, 1H), 4.08 (q, *J* = 6.4 Hz, 1H), 1.17 (d, *J* = 6.4 Hz, 6H); HRMS (ESI-Orbitrap) Calcd for C₂₀H₂₂N₅O₂: 364.1773 [M+H⁺], Found 364.1792.

***N*-Isopropyl-3-(3-(4-(pyridin-4-yl)phenyl)ureido)benzamide (7b)**—65% yield in 3 steps. ¹H-NMR (DMSO-*d*₆, 400 MHz) δ 9.12 (s, 1H), 9.04 (s, 1H), 8.78 (d, *J* = 5.6 Hz, 2H), 8.19–8.17 (m, 1H), 8.12 (d, *J* = 5.6 Hz, 2H), 7.96 (d, *J* = 8.8 Hz, 2H), 7.89–7.88 (m, 1H), 7.70 (d, *J* = 8.8 Hz, 2H), 7.64–7.61 (m, 1H), 7.46–7.44 (m, 1H), 7.38–7.34 (m, 1H), 4.08 (q, *J* = 6.4 Hz, 1H), 1.17 (d, *J* = 6.4 Hz, 6H); ¹³C-NMR (DMSO-*d*₆, 100 MHz) δ 165.46, 152.57, 152.35, 144.23, 142.99, 139.46, 135.77, 128.52, 128.49, 127.52, 121.84, 120.82, 120.68, 118.42, 117.74, 40.94, 22.28; LC/MS (M+H⁺): 375.14.

3-(3-(4-(2-Aminopyrimidin-4-yl)phenyl)ureido)-*N*-isopropylbenzamide (7c)—52% yield in 4 steps. ¹H-NMR (DMSO-*d*₆, 400 MHz) δ 9.43 (s, br, 2H), 8.92–8.80 (m, 1H), 8.32–8.17 (m, 1H), 8.24–8.17 (m, 1H), 8.12–8.10 (m, 2H), 7.90 (s, 1H), 7.66–7.61 (m, 3H), 7.45–7.34 (m, 3H), 7.28 (s, 1H), 4.09 (q, *J* = 6.8 Hz, 1H), 1.16 (d, *J* = 6.8 Hz, 6H); ¹³C-NMR (DMSO-*d*₆, 100 MHz) δ 166.79, 165.51, 159.06, 152.36, 152.00, 143.87, 139.51, 135.78, 128.67, 128.46, 128.19, 120.74, 120.66, 117.72, 117.64, 105.05, 40.93, 22.27; HRMS (ESI-Orbitrap) Calcd for C₂₁H₂₃N₅O₂: 391.1882 [M+H⁺], Found 391.1889.

***N*-Isopropyl-4-[3-[4-(1*H*-pyrrolo[2,3-*b*]pyridin-4-yl)-phenyl]-ureido]-benzamide (7d)**—40% yield in 4 steps. ¹H-NMR (DMSO-*d*₆, 400 MHz) δ 12.26 (s, br, 1H), 9.08 (s, 1H), 8.97 (s, 1H), 8.80 (s, 1H), 8.25–8.14 (m, 3H), 8.12 (d, *J* = 8.8 Hz, 2H), 7.87 (s, 1H), 7.76 (d, *J* = 8.8 Hz, 2H), 7.46–6.36 (m, 2H), 6.96–6.95 (m, 2H), 4.08 (m, 1H), 1.17 (d, *J* = 6.4 Hz, 6H); LC/MS (M+H⁺): 414.15.

4-[3-[4-(7-Ethyl-8-oxo-8,9-dihydro-7*H*-purin-6-yl)-phenyl]-ureido]-*N*-isopropylbenzamide (7e)—45% yield in 4 steps. ¹H-NMR (DMSO-*d*₆, 400 MHz) δ 12.08 (s, br, 1H), 9.42 (s, 1H), 8.84–8.82 (m, 1H), 8.76 (s, 1H), 8.35–8.14 (m, 3H), 8.12 (d, *J* = 8.8 Hz,

2H), 7.96 (d, $J = 8.8$ Hz, 2H), 7.69–7.59 (m, 1H), 4.08 (m, 1H), 3.35 (q, $J = 3.2$ Hz, 2H), 1.17 (d, $J = 6.4$ Hz, 6H), 1.07 (t, $J = 3.2$ Hz, 3H); LC/MS ($M+H^+$): 460.17.

***N*-Isopropyl-4-[3-[4-(9*H*-purin-6-yl)-phenyl]-ureido]-benzamide (7f)**—29% yield in 4 steps. $^1\text{H-NMR}$ (DMSO- d_6 , 400 MHz) δ 11.98. (s, br, 1H), 9.48 (s, 1H), 8.81–8.79 (m, 1H), 8.76 (s, 1H), 8.35–8.14 (m, 3H), 8.12 (d, $J = 8.8$ Hz, 2H), 7.96 (d, $J = 8.8$ Hz, 2H), 7.69–7.59 (m, 2H), 6.95 (s, 1H), 4.08 (m, 1H), 1.17 (d, $J = 6.4$ Hz, 6H); HRMS (ESI-Orbitrap) Calcd for $C_{22}H_{22}N_7O_2$: 416.1835 [$M+H^+$], Found 416.1849.

***N*-Isopropyl-3-(3-(4-(5-methyl-7*H*-pyrrolo[2,3-*d*]pyrimidin-4-yl)phenyl)ureido)benzamide (7g)**—40% yield in 4 steps. $^1\text{H-NMR}$ (DMSO- d_6 , 400 MHz) δ 12.63 (s, 1H), 9.21 (s, 1H), 9.10 (s, 1H), 8.92 (s, 1H), 8.19–8.18 (m, 1H), 7.89 (s, 1H), 7.74–7.68 (m, 4H), 7.65–7.61 (m, 2H), 7.46–7.44 (m, 1H), 7.39–7.35 (m, 1H), 4.10 (q, $J = 6.4$ Hz, 1H), 2.10 (s, 3H), 1.17 (d, $J = 6.4$ Hz, 6H); $^{13}\text{C-NMR}$ (DMSO- d_6 , 100 MHz) δ 165.52, 159.07, 158.74, 153.86, 152.50, 152.09, 145.81, 142.76, 139.59, 135.78, 130.90, 128.46, 125.16, 120.78, 117.71, 117.44, 114.54, 111.64, 40.94, 22.27, 12.51; HRMS (ESI-Orbitrap) Calcd for $C_{24}H_{25}N_6O_2$: 429.2039 [$M+H^+$], Found 429.2029.

***N*-Isopropyl-3-(3-(4-(6-methyl-7*H*-pyrrolo[2,3-*d*]pyrimidin-4-yl)phenyl)ureido)benzamide (7h)**—35% yield in 4 steps. $^1\text{H-NMR}$ (DMSO- d_6 , 400 MHz) δ 12.22 (s, br, 1H), 9.07 (s, 1H), 8.96 (s, 1H), 8.74 (s, 1H), 8.20–8.18 (m, 1H), 8.14–8.12 (m, 2H), 7.88 (s, 1H), 7.70–7.68 (m, 2H), 7.66–7.61 (m, 1H), 7.46–7.44 (m, 1H), 7.38–7.34 (m, 1H), 6.69 (s, 1H), 4.10 (q, $J = 6.8$ Hz, 1H), 1.17 (d, $J = 6.8$ Hz, 6H); LC/MS ($M+H^+$): 429.17.

3-(3-(4-(5,6-Dimethyl-7*H*-pyrrolo[2,3-*d*]pyrimidin-4-yl)phenyl)ureido)-*N*-isopropylbenzamide (7i)—32% yield in 4 steps. $^1\text{H-NMR}$ (DMSO- d_6 , 400 MHz) δ 9.04 (s, 1H), 8.99 (s, 1H), 8.74–8.73 (m, 1H), 8.19–8.17 (m, 1H), 7.87 (s, 1H), 7.68–7.61 (m, 5H), 7.46–7.44 (m, 1H), 7.38–7.34 (m, 1H), 4.11 (q, $J = 6.8$ Hz, 1H), 1.97 (s, 3H), 1.17 (d, $J = 6.8$ Hz, 6H); LC/MS ($M+H^+$): 443.16.

3-(3-(2-(2-(Dimethylamino)ethoxy)-4-(5-methyl-7*H*-pyrrolo[2,3-*d*]pyrimidin-4-yl)phenyl)ureido)-*N*-isopropylbenzamide (7l)—46% yield in 4 steps. $^1\text{H-NMR}$ (DMSO- d_6 , 400 MHz) δ 12.3 (s, br, 1H), 9.73 (s, 1H), 9.60 (s, 1H), 8.84 (s, 1H), 8.45 (s, 1H), 8.34–8.32 (m, 1H), 8.20–8.18 (m, 1H), 7.90 (s, 1H), 7.71–7.70 (m, 1H), 7.51 (s, 1H), 7.48–7.47 (m, 1H), 7.40–7.33 (m, 2H), 4.51 (t, $J = 4.6$ Hz, 2H), 4.10 (q, $J = 6.4$ Hz, 1H), 3.63 (t, $J = 4.6$ Hz, 2H), 2.94 (s, 6H), 2.12 (s, 3H), 1.17 (d, $J = 6.4$ Hz, 6H); $^{13}\text{C-NMR}$ (DMSO- d_6 , 100 MHz) δ 165.44, 158.91, 158.58, 154.45, 152.33, 152.23, 146.68, 145.76, 139.52, 135.78, 131.26, 128.52, 127.95, 123.80, 120.68, 118.34, 117.72, 114.64, 113.18, 111.10, 62.96, 55.44, 42.65, 40.94, 22.26, 12.78; LC/MS ($M+H^+$): 516.13.

***N*-Isopropyl-3-(3-(4-(5-methyl-7*H*-pyrrolo[2,3-*d*]pyrimidin-4-yl)-2-(trifluoromethyl)phenyl)ureido)-benzamide (7j)**—47% yield in 4 steps. $^1\text{H-NMR}$ (DMSO- d_6 , 400 MHz) δ 12.19 (s, br, 1H), 9.71 (s, 1H), 8.83 (s, 1H), 8.33–8.26 (m, 2H), 8.21–8.19 (m, 1H), 8.01–8.00 (m, 2H), 7.85 (s, 1H), 7.70–7.68 (m, 1H), 7.48–7.46 (m, 2H), 7.41–7.37 (m, 1H), 4.10 (q, $J = 6.8$ Hz, 1H), 2.09 (s, 3H), 1.16 (d, $J = 6.8$ Hz, 6H); ^{13}C -

NMR (DMSO- d_6 , 100 MHz) δ 165.37, 155.31, 152.57, 152.17, 149.46, 139.24, 137.50, 135.83, 134.08, 131.87, 128.70, 127.18, 126.48, 125.15, 124.24, 122.44, 120.96, 120.58, 117.53, 114.95, 108.93, 40.93, 22.27, 12.81; HRMS (ESI-Orbitrap), Calcd for $C_{25}H_{24}F_3N_6O_2$: 497.1913 [M+H⁺], Found 497.1902.

3-(3-(2-Fluoro-4-(5-methyl-7H-pyrrolo[2,3-d]pyrimidin-4-yl)phenyl)ureido)-N-isopropylbenzamide (7k)—42% yield in 4 steps. ¹H-NMR (DMSO- d_6 , 400 MHz) δ 12.20 (s, br, 1H), 9.46 (s, 1H), 8.89 (s, 1H), 8.81 (s, 1H), 8.52–8.49 (m, 1H), 8.25–8.19 (m, 1H), 7.88–7.84 (m, 1H), 7.68–7.64 (m, 2H), 7.52–7.48 (m, 3H), 7.42–7.39 (m, 1H), 4.10 (q, J = 6.8 Hz, 1H), 2.10 (s, 3H), 1.17 (d, J = 6.8 Hz, 6H); ¹³C-NMR (DMSO- d_6 , 100 MHz) δ 165.44, 154.88, 152.40, 152.10, 149.96, 148.37, 139.27, 135.83, 129.21, 128.61, 126.88, 126.43, 120.84, 120.56, 119.50, 117.45, 116.19, 115.99, 114.82, 109.82, 40.95, 22.26, 12.75; HRMS (ESI-Orbitrap), Calcd for $C_{24}H_{24}FN_6O_2$: 447.1945 [M+H⁺], Found 447.1934.

1-(4-(5-Methyl-7H-pyrrolo[2,3-d]pyrimidin-4-yl)phenyl)-3-phenylurea (10a)—62% yield in 3 steps. ¹H-NMR (DMSO- d_6 , 400 MHz) δ 12.56 (s, br, 1H), 9.18 (s, 1H), 8.94–8.90 (m, 2H), 7.78–7.67 (m, 4H), 7.62–7.58 (m, 1H), 7.50–7.48 (m, 2H), 7.32–7.28 (m, 2H), 7.01–6.98 (m, 1H), 2.10 (s, 3H); HRMS, Calcd for $C_{20}H_{18}N_5O$: 344.1511 [M+H⁺], Found 344.1526.

1-(3-Fluorophenyl)-3-(4-(5-methyl-7H-pyrrolo[2,3-d]pyrimidin-4-yl)phenyl)urea (10b)—51% yield in 3 steps. ¹H-NMR (DMSO- d_6 , 400 MHz) δ 12.55 (s, br, 1H), 9.17–9.12 (m, 2H), 8.88 (s, 1H), 7.69–7.68 (m, 4H), 7.60–7.50 (m, 2H), 7.36–7.31 (m, 1H), 7.18–7.16 (m, 1H), 6.84–6.79 (m, 1H), 2.10 (s, 3H); LC/MS (M+H⁺): 362.11.

1-(2-Methoxyphenyl)-3-(4-(5-methyl-7H-pyrrolo[2,3-d]pyrimidin-4-yl)phenyl)urea (10c)—60% yield in 3 steps. ¹H-NMR (DMSO- d_6 , 400 MHz) δ 12.49 (s, 1H), 9.66 (s, 1H), 8.88 (s, 1H), 8.35 (s, 1H), 8.16–8.14 (m, 1H), 7.69–7.68 (m, 4H), 7.56 (s, 1H), 7.06–7.03 (m, 1H), 7.00–6.98 (m, 1H), 6.96–6.89 (m, 1H), 3.90 (s, 3H), 2.10 (s, 3H); ¹³C-NMR (DMSO- d_6 , 100 MHz) δ 154.87, 152.24, 152.18, 147.80, 146.90, 142.24, 130.81, 128.35, 127.60, 126.70, 122.12, 120.52, 118.45, 117.12, 114.61, 110.93, 110.77, 55.75, 12.66; LC/MS (M+H⁺): 374.09.

1-(3-Methoxyphenyl)-3-(4-(5-methyl-7H-pyrrolo[2,3-d]pyrimidin-4-yl)phenyl)urea (10d)—57% yield in 3 steps. ¹H-NMR (DMSO- d_6 , 400 MHz) δ 12.61 (s, br, 1H), 9.14 (s, 1H), 8.93–8.91 (m, 2H), 7.72–7.67 (m, 4H), 7.60 (s, 1H), 7.23–7.18 (m, 2H), 6.98–6.96 (m, 1H), 6.59–6.57 (m, 1H), 3.74 (s, 3H), 2.10 (s, 3H); ¹³C-NMR (DMSO- d_6 , 100 MHz) δ 159.64, 153.71, 152.42, 152.07, 145.64, 142.89, 140.85, 130.91, 129.49, 128.52, 124.83, 117.37, 114.51, 111.75, 110.63, 107.32, 104.13, 54.88, 12.50; LC/MS (M+H⁺): 374.09.

1-(4-Methoxyphenyl)-3-(4-(5-methyl-7H-pyrrolo[2,3-d]pyrimidin-4-yl)phenyl)urea (10e)—45% yield in 3 steps. ¹H-NMR (DMSO- d_6 , 400 MHz) δ 11.89 (s, br, 1H), 8.86 (s, 1H), 8.71 (s, 1H), 8.60 (s, 1H), 7.61–7.60 (m, 4H), 7.38 (d, J = 8.8 Hz, 2H),

7.35 (s, 1H), 6.88 (d, $J = 8.8$ Hz, 2H), 3.73 (s, 3H), 2.10 (s, 3H); LC/MS ($M+H^+$): 374.14; HRMS (ESI-Orbitrap) Calcd for $C_{21}H_{20}N_5O_2$: 374.1617 [$M+H^+$], Found 374.1608.

1-[4-(5-Methyl-7H-pyrrolo[2,3-d]pyrimidin-4-yl)-phenyl]-3-thiazol-2-yl-urea (10f)

—40% yield in 3 steps. 1H -NMR (DMSO- d_6 , 400 MHz) δ 11.95 (s, br, 1H), 8.76 (s, 1H), 8.71 (s, 1H), 8.60 (s, 1H), 7.71–7.68 (m, 4H), 7.53–7.48 (m, 1H), 6.99–6.97 (m, 1H), 6.58–6.56 (m, 1H), 2.10 (s, 3H); LC/MS ($M+H^+$): 351.14.

1-[4-(5-Methyl-7H-pyrrolo[2,3-d]pyrimidin-4-yl)-phenyl]-3-pyridin-2-yl-urea (10g)—48% yield in 3 steps. LC/MS ($M+H^+$): 345.12.

3-(4-Methoxyphenyl)-1-methyl-1-(4-(5-methyl-7H-pyrrolo[2,3-d]pyrimidin-4-yl)phenyl)urea (14a)—55% yield in 3 steps. 1H -NMR (DMSO- d_6 , 400 MHz) δ 12.40 (s, br, 1H), 8.87 (s, 1H), 8.40 (s, 1H), 7.73 (d, $J = 8.8$ Hz, 2H), 7.55–7.54 (m, 1H), 7.52 (d, $J = 8.8$ Hz, 2H), 7.36 (d, $J = 6.8$ Hz, 2H), 6.85 (d, $J = 6.8$ Hz, 2H), 3.38 (s, 3H), 3.17 (s, 3H), 2.11 (s, 3H); ^{13}C -NMR (DMSO- d_6 , 100 MHz) δ 159.21, 154.89, 152.28, 147.29, 146.42, 134.02, 132.78, 130.47, 127.57, 127.29, 124.54, 122.05, 114.80, 113.53, 110.66, 55.12, 37.10, 12.67; LC/MS ($M+H^+$): 388.18; HRMS (ESI-Orbitrap) Calcd for $C_{22}H_{22}N_5O_2$: 388.1773 [$M+H^+$], Found 388.1764.

3-(4-Methoxyphenyl)-1-(4-(5-methyl-7H-pyrrolo[2,3-d]pyrimidin-4-yl)phenyl)-1-(2-(pyrrolidin-1-yl)ethyl)urea (14b)—18% yield in 5 steps. 1H -NMR (DMSO- d_6 , 400 MHz) δ 9.59 (s, br, 1H), 8.79 (s, 1H), 8.12 (s, 1H), 7.80 (d, $J = 8.4$ Hz, 2H), 7.57 (d, $J = 8.4$ Hz, 2H), 7.43 (s, 1H), 7.32 (d, $J = 6.8$ Hz, 2H), 6.82 (d, $J = 6.8$ Hz, 2H), 4.08–4.04 (m, 2H), 3.70 (s, 3H), 3.65–3.64 (m, 2H), 3.37–3.32 (m, 2H), 3.12–3.06 (m, 2H), 2.14 (s, 3H), 2.04–2.02 (m, 2H), 1.90–1.86 (m, 2H); HRMS (ESI-Orbitrap), Calcd for $C_{27}H_{31}N_6O_2$: 471.2508 [$M+H^+$], Found 471.2516.

3-(4-Methoxyphenyl)-1-(4-(5-methyl-7H-pyrrolo[2,3-d]pyrimidin-4-yl)phenyl)-1-(2-(piperidin-1-yl)ethyl)urea (14c)—19% yield in 5 steps. 1H -NMR (DMSO- d_6 , 400 MHz) δ 12.02 (s, br, 1H), 8.77 (s, 1H), 8.15 (s, 1H), 7.80 (d, $J = 8.4$ Hz, 2H), 7.56 (d, $J = 8.4$ Hz, 2H), 7.41 (s, 1H), 7.31 (d, $J = 8.8$ Hz, 2H), 6.83 (d, $J = 8.8$ Hz, 2H), 4.09–4.06 (m, 2H), 3.70 (s, 3H), 3.56–3.54 (m, 2H), 3.28–3.24 (m, 2H), 2.97–2.91 (m, 2H), 2.14 (s, 3H), 1.85–1.81 (m, 2H), 1.68–1.62 (m, 4H); LC/MS ($M+H^+$): 485.15.

3-(4-(5-Methyl-7H-pyrrolo[2,3-d]pyrimidin-4-yl)phenyl)-1-phenyl-1-(2-(pyrrolidin-1-yl)ethyl)urea (18a)—46% yield in 4 steps. 1H NMR (DMSO- d_6 , 400 MHz) δ 12.04 (s, br, 1H), 9.57 (s, 1H), 8.74 (s, 1H), 8.20 (s, 1H), 7.63–7.55 (m, 4H), 7.53–7.51 (m, 2H), 7.48–7.46 (m, 1H), 7.42–7.39 (m, 2H), 4.04–4.00 (m, 2H), 3.68–3.65 (m, 2H), 3.31–3.29 (m, 2H), 3.08–3.07 (m, 2H), 2.04–2.02 (m, 5H), 1.90–1.87 (m, 2H); LC/MS ($M+H^+$): 441.00.

1-(2-Hydroxyethyl)-3-(4-(5-methyl-7H-pyrrolo[2,3-d]pyrimidin-4-yl)phenyl)-1-phenylurea (18b)—From commercially available 2-phenylamino-ethanol, **18b** was synthesized in 62% yield through 3 steps. 1H -NMR (DMSO- d_6 , 400 MHz) δ 8.83–8.81 (m, 1H), 8.40 (s, 1H), 7.64–7.58 (m, 4H), 7.47–7.43 (m, 3H), 7.39–7.37 (m, 2H), 7.32–7.29 (m,

1H), 3.76 (t, $J = 6.4$ Hz, 2H), 3.56 (t, $J = 6.4$ Hz, 2H), 2.06 (s, 3H); ^{13}C -NMR (DMSO- d_6 , 100 MHz) δ 154.43, 152.14, 146.62, 142.62, 130.30, 129.37, 129.09, 127.78, 127.66, 127.59, 126.52, 119.18, 118.67, 114.56, 111.08, 58.79, 52.24, 12.61; HRMS (ESI-Orbitrap), Calcd for $\text{C}_{22}\text{H}_{22}\text{N}_5\text{O}_2$: 388.1773 [$\text{M}+\text{H}^+$], Found 388.1764.

1-(2-Fluorophenyl)-1-(2-hydroxyethyl)-3-(4-(5-methyl-7H-pyrrolo[2,3-d]pyrimidin-4-yl)phenyl)urea (18c)—49% yield in 5 steps. ^1H -NMR (DMSO- d_6 , 400 MHz) δ 12.59 (s, br, 1H), 8.89 (s, 1H), 8.75 (s, 1H), 7.66–7.54 (m, 4H), 7.52–7.50 (m, 1H), 7.42–7.40 (m, 1H), 7.39–7.37 (m, 1H), 7.34–7.26 (m, 2H), 3.72 (t, $J = 6.4$ Hz, 2H), 3.57 (t, $J = 6.4$ Hz, 2H), 2.07 (s, 3H); ^{13}C -NMR (DMSO- d_6 , 100 MHz) δ 159.17, 158.37, 156.71, 154.39, 153.62, 152.07, 145.55, 143.00, 130.74, 130.49, 129.81, 128.64, 125.11, 119.20, 116.55, 114.51, 111.76, 58.92, 51.98, 12.47; LC/MS ($\text{M}+\text{H}^+$): 406.07.

1-(3-Fluorophenyl)-1-(2-hydroxyethyl)-3-(4-(5-methyl-7H-pyrrolo[2,3-d]pyrimidin-4-yl)phenyl)urea (18d)—45% yield in 5 steps. ^1H -NMR (DMSO- d_6 , 400 MHz) δ 12.54 (s, br, 1H), 8.88 (s, 1H), 8.66 (s, 1H), 7.68–7.62 (m, 4H), 7.57 (s, 1H), 7.48–7.43 (m, 1H), 7.32–7.29 (m, 1H), 7.23–7.21 (m, 1H), 7.15–7.10 (m, 1H), 3.79 (t, $J = 6.0$ Hz, 2H), 3.58 (t, $J = 6.0$ Hz, 2H), 2.07 (s, 3H); ^{13}C -NMR (DMSO- d_6 , 100 MHz) δ 163.53, 161.11, 154.21, 152.14, 146.34, 144.40, 142.65, 130.67, 130.58, 130.36, 128.04, 123.44, 118.83, 114.75, 114.52, 112.97, 111.26, 58.81, 52.25, 12.58; HRMS (ESI-Orbitrap), Calcd for $\text{C}_{22}\text{H}_{21}\text{FN}_5\text{O}_2$: 406.1679 [$\text{M}+\text{H}^+$], Found 406.1686.

1-(4-Fluorophenyl)-1-(2-hydroxyethyl)-3-(4-(5-methyl-7H-pyrrolo[2,3-d]pyrimidin-4-yl)phenyl)urea (18e)—41% yield in 5 steps. ^1H -NMR (DMSO- d_6 , 400 MHz) δ 12.51 (s, br, 1H), 8.86 (s, 1H), 8.37 (s, 1H), 7.66–7.62 (m, 4H), 7.60 (s, 1H), 7.44–7.41 (m, 2H), 7.29–7.25 (m, 2H), 3.73 (t, $J = 6.0$ Hz, 2H), 3.55 (t, $J = 6.0$ Hz, 2H), 2.06 (s, 3H); ^{13}C -NMR (DMSO- d_6 , 100 MHz) δ 161.76, 159.34, 154.39, 152.13, 146.35, 142.72, 138.65, 130.30, 130.14, 128.01, 118.83, 116.20, 115.98, 114.55, 111.24, 58.70, 52.33, 12.57; LC/MS ($\text{M}+\text{H}^+$): 406.06; HRMS (ESI-Orbitrap), Calcd for $\text{C}_{22}\text{H}_{21}\text{FN}_5\text{O}_2$: 406.1679 [$\text{M}+\text{H}^+$], Found 406.1670.

1-(2-Chlorophenyl)-1-(2-hydroxyethyl)-3-(4-(5-methyl-7H-pyrrolo[2,3-d]pyrimidin-4-yl)phenyl)urea (18f)—40% yield in 5 steps. ^1H -NMR (DMSO- d_6 , 400 MHz) δ 12.70 (s, br, 1H), 8.92 (s, 1H), 8.72 (s, 1H), 7.69–7.63 (m, 5H), 7.53–7.52 (m, 1H), 7.47–7.43 (m, 1H), 7.36–7.33 (m, 1H), 3.78 (t, $J = 6.0$ Hz, 2H), 3.57 (t, $J = 6.0$ Hz, 2H), 2.07 (s, 3H); ^{13}C -NMR (DMSO- d_6 , 100 MHz) δ 158.42, 158.07, 154.22, 152.08, 145.63, 144.25, 142.95, 133.22, 130.69, 130.46, 128.58, 127.53, 126.23, 126.19, 118.86, 114.51, 111.70, 58.82, 52.31, 12.49; HRMS (ESI-Orbitrap), Calcd for $\text{C}_{22}\text{H}_{21}\text{ClN}_5\text{O}_2$: 422.1384 [$\text{M}+\text{H}^+$], Found 422.1369.

1-(3-Chlorophenyl)-1-(2-hydroxyethyl)-3-(4-(5-methyl-7H-pyrrolo[2,3-d]pyrimidin-4-yl)phenyl)urea (18g)—45% yield in 5 steps. ^1H -NMR (DMSO- d_6 , 400 MHz) δ 8.85 (s, 1H), 7.64–7.58 (m, 5H), 7.57–7.56 (m, 1H), 7.52 (s, 1H), 7.47–7.45 (m, 1H), 7.44–7.39 (m, 2H), 3.58 (t, $J = 6.0$ Hz, 2H), 3.42 (t, $J = 6.0$ Hz, 2H), 2.06 (s, 3H); ^{13}C -NMR (DMSO- d_6 , 100 MHz) δ 158.28, 157.95, 154.22, 152.12, 146.21, 142.75, 139.25,

132.59, 131.76, 130.35, 130.24, 129.21, 128.36, 128.15, 118.99, 114.53, 111.33, 58.79, 51.67, 12.58; LC/MS (M+H⁺): 422.06.

1-(4-Chlorophenyl)-1-(2-hydroxyethyl)-3-(4-(5-methyl-7H-pyrrolo[2,3-d]pyrimidin-4-yl)phenyl)urea (18h)—48% yield in 5 steps. ¹H-NMR (DMSO-d₆, 400 MHz) δ 12.49 (s, br, 1H), 8.87 (s, 1H), 8.56 (s, 1H), 7.66–7.60 (m, 4H), 7.55 (s, 1H), 7.50–7.47 (m, 2H), 7.43–7.40 (m, 2H), 3.75 (t, *J* = 6.0 Hz, 2H), 3.56 (t, *J* = 6.0 Hz, 2H), 2.06 (s, 3H); HRMS (ESI-Orbitrap), Calcd for C₂₂H₂₁ClN₅O₂: 422.1384 [M+H⁺], Found 422.1375.

1-(2-Hydroxyethyl)-3-(4-(5-methyl-7H-pyrrolo[2,3-d]pyrimidin-4-yl)phenyl)-1-*o*-tolylurea (18i)—45% yield in 5 steps. ¹H-NMR (DMSO-d₆, 400 MHz) δ 12.56 (s, br, 1H), 8.88 (s, 1H), 8.18 (s, 1H), 7.65–7.58 (m, 5H), 7.36–7.29 (m, 4H), 3.74 (t, *J* = 6.0 Hz, 2H), 3.58 (t, *J* = 6.0 Hz, 2H), 2.22 (s, 3H), 2.06 (s, 3H); ¹³C-NMR (DMSO-d₆, 100 MHz) δ 158.40, 158.06, 154.37, 153.84, 152.08, 145.75, 143.02, 136.21, 131.13, 130.43, 129.30, 128.47, 127.64, 127.09, 118.82, 114.50, 111.62, 58.82, 51.71, 17.31, 12.51; LC/MS (M+H⁺): 402.09.

1-(2-Hydroxyethyl)-3-(4-(5-methyl-7H-pyrrolo[2,3-d]pyrimidin-4-yl)phenyl)-1-*m*-tolylurea (18j)—43% yield in 5 steps. ¹H-NMR (DMSO-d₆, 400 MHz) δ 12.70 (s, br, 1H), 8.92 (s, 1H), 8.40 (s, 1H), 7.68–7.61 (m, 5H), 7.35–7.31 (m, 1H), 7.21 (s, 1H), 7.16–7.12 (m, 2H), 3.74 (t, *J* = 6.4 Hz, 2H), 3.53 (t, *J* = 6.4 Hz, 2H), 2.35 (s, 3H), 2.07 (s, 3H); ¹³C-NMR (DMSO-d₆, 100 MHz) δ 158.11, 154.38, 153.97, 152.09, 145.87, 142.96, 142.34, 138.77, 130.42, 129.16, 128.37, 128.20, 127.32, 124.73, 118.69, 114.50, 111.55, 58.75, 52.20, 20.95, 12.53; LC/MS (M+H⁺): 402.06.

1-(2-Hydroxyethyl)-3-(4-(5-methyl-7H-pyrrolo[2,3-d]pyrimidin-4-yl)phenyl)-1-*p*-tolylurea (18k)—39% yield in 5 steps. ¹H-NMR (DMSO-d₆, 400 MHz) δ 12.60 (s, br, 1H), 8.89 (s, 1H), 8.28 (s, 1H), 7.66–7.62 (m, 4H), 7.60–7.58 (m, 1H), 7.26–7.25 (m, 4H), 3.72 (t, *J* = 6.0 Hz, 2H), 3.54 (t, *J* = 6.0 Hz, 2H), 2.34 (s, 3H), 2.07 (s, 3H); LC/MS (M+H⁺): 402.09; HRMS (ESI-Orbitrap) Calcd for C₂₃H₂₄N₅O₂: 402.1930 [M+H⁺], Found 402.1920.

1-(2-Hydroxyethyl)-1-(2-methoxyphenyl)-3-(4-(5-methyl-7H-pyrrolo[2,3-d]pyrimidin-4-yl)phenyl)urea (18l)—47% yield in 5 steps. ¹H-NMR (DMSO-d₆, 400 MHz) δ 8.83 (s, 1H), 7.59–7.58 (m, 5H), 7.49–7.48 (m, 1H), 7.38–7.32 (m, 2H), 7.16–7.14 (m, 1H), 7.04–7.00 (m, 1H), 3.80 (s, 3H), 3.62–3.51 (m, 4H), 2.06 (s, 3H); ¹³C-NMR (DMSO-d₆, 100 MHz) δ 158.30, 155.25, 154.72, 154.23, 152.10, 146.10, 143.02, 130.49, 130.32, 130.01, 128.97, 128.16, 120.86, 118.67, 114.51, 112.74, 111.39, 58.74, 55.67, 51.22, 12.54; LC/MS (M+H⁺): 418.07.

1-(2-Hydroxyethyl)-1-(3-methoxyphenyl)-3-(4-(5-methyl-7H-pyrrolo[2,3-d]pyrimidin-4-yl)phenyl)urea (18m)—46% yield in 5 steps. ¹H-NMR (DMSO-d₆, 400 MHz) δ 12.50 (s, br, 1H), 8.86 (s, 1H), 8.39 (s, 1H), 7.66–7.60 (m, 4H), 7.55 (s, 1H), 7.36–7.32 (m, 1H), 6.98–6.97 (m, 1H), 6.93–6.88 (m, 2H), 3.78 (s, 3H), 3.75 (t, *J* = 6.0 Hz, 2H), 3.56 (t, *J* = 6.0 Hz, 2H), 2.07 (s, 3H); ¹³C-NMR (DMSO-d₆, 100 MHz) δ 159.95, 158.32, 158.10, 154.26, 152.11, 146.22, 143.55, 142.78, 130.36, 130.05, 128.11, 119.77,

118.71, 114.53, 113.57, 112.22, 111.33, 58.75, 55.18, 52.19, 12.57; LC/MS (M+H⁺): 418.05.

1-(2-hydroxyethyl)-1-(4-methoxyphenyl)-3-(4-(5-methyl-7H-pyrrolo[2,3-d]pyrimidin-4-yl)phenyl)urea (18n)—48% yield in 5 steps. ¹H-NMR (DMSO-d₆, 400 MHz) δ 12.56 (s, br, 1H), 8.88 (s, 1H), 8.13 (s, 1H), 7.66–7.59 (m, 5H), 7.30 (d, *J* = 6.8 Hz, 2H), 7.01 (d, *J* = 6.8 Hz, 2H), 3.80 (s, 3H), 3.69 (t, *J* = 6.4 Hz, 2H), 3.53 (t, *J* = 6.4 Hz, 2H), 2.06 (s, 3H); HRMS (ESI-Orbitrap), Calcd for C₂₃H₂₄N₅O₃: 418.1879 [M+H⁺], Found 418.1686.

1-(2-Aminoethyl)-1-(4-methoxyphenyl)-3-(4-(5-methyl-7H-pyrrolo[2,3-d]pyrimidin-4-yl)phenyl)urea (18o)—52% yield in 4 steps. ¹H-NMR (DMSO-d₆, 400 MHz) δ 12.64 (s, 1H), 8.86 (s, 1H), 8.35 (s, 1H), 7.82 (s, 2H), 7.59 (dt, *J* = 13.0, 6.5 Hz, 5H), 7.53 – 7.43 (m, 4H), 3.85 (t, *J* = 6.2 Hz, 2H), 2.93 – 2.82 (m, 2H), 2.00 (dd, *J* = 8.4, 2.5 Hz, 3H). LC/MS (M+H⁺): 415.11.

1-(2-Aminoethyl)-1-(4-chlorophenyl)-3-(4-(5-methyl-7H-pyrrolo[2,3-d]pyrimidin-4-yl)phenyl)urea (18p)—45% yield in 4 steps. ¹H-NMR (DMSO-d₆, 400 MHz) δ 12.60 (s, 1H), 8.89 (s, 1H), 8.06 (s, 1H), 7.87 (s, 2H), 7.69 (d, *J* = 8.8 Hz, 2H), 7.62 (d, *J* = 8.8 Hz, 2H), 7.58 (s, 1H), 7.45 – 7.39 (m, 2H), 7.10 – 7.04 (m, 2H), 3.87 (t, *J* = 6.2 Hz, 2H), 3.81 (d, *J* = 9.0 Hz, 3H), 2.99 – 2.88 (m, 2H), 2.06 (d, *J* = 0.9 Hz, 3H). HRMS (ESI-Orbitrap), Calcd for C₂₂H₂₂ClN₅O: 421.1544 [M+H⁺], Found 421.1563.

1-(2-(Dimethylamino)ethyl)-1-(4-methoxyphenyl)-3-(4-(5-methyl-7H-pyrrolo[2,3-d]pyrimidin-4-yl)phenyl)urea (18q)—50% yield in 4 steps. ¹H-NMR (DMSO-d₆, 400 MHz) δ 12.55 (s, 1H), 9.42 (s, 1H), 8.88 (s, 1H), 8.10 (s, 1H), 7.69 (d, *J* = 8.8 Hz, 2H), 7.62 (d, *J* = 8.8 Hz, 2H), 7.57 (s, 1H), 7.45 – 7.38 (m, 2H), 7.11 – 7.03 (m, 2H), 3.98 (t, *J* = 6.2 Hz, 2H), 3.82 (s, 3H), 3.20 (d, *J* = 5.2 Hz, 2H), 2.88 (t, *J* = 8.5 Hz, 6H), 2.05 (d, *J* = 0.9 Hz, 3H). LC/MS (ESI-Orbitrap), Found 445.21.

1-(4-Chlorophenyl)-1-(2-(dimethylamino)ethyl)-3-(4-(5-methyl-7H-pyrrolo[2,3-d]pyrimidin-4-yl)phenyl)urea (18r)—65% yield in 4 steps. ¹H-NMR (DMSO-d₆, 400 MHz) δ 12.70 (s, 1H), 9.52 (s, 1H), 8.93 (s, 1H), 8.48 (s, 0H), 7.67 (dd, *J* = 23.4, 8.8 Hz, 4H), 7.62 – 7.49 (m, 5H), 4.04 (t, *J* = 6.2 Hz, 2H), 3.21 (d, *J* = 4.7 Hz, 2H), 2.89 (d, *J* = 3.5 Hz, 6H), 2.06 (d, *J* = 0.7 Hz, 3H). LC/MS (ESI-Orbitrap), Found 449.21.

1-(4-Chlorophenyl)-3-(4-(5,6-dimethyl-7H-pyrrolo[2,3-d]pyrimidin-4-yl)-2-fluorophenyl)-1-(2-hydroxyethyl)urea (18s)—52% yield in 4 steps. ¹H-NMR (DMSO-d₆, 400 MHz) δ 12.67 (s, 1H), 8.84 (s, 1H), 8.54 (s, 1H), 7.93 (t, *J* = 8.3 Hz, 1H), 7.58 (dd, *J* = 11.4, 1.9 Hz, 2H), 7.54 – 7.40 (m, 4H), 3.80 – 3.76 (m, 4H), 2.40 (d, *J* = 10.5 Hz, 3H), 1.93 (s, 3H). HRMS (ESI-Orbitrap) Calcd for C₂₃H₂₁ClFN₅O₂: 454.1446 [M+H⁺], Found 454.1434.

1-(2-Amino-ethyl)-1-(4-chloro-phenyl)-3-[4-(5,6-dimethyl-7H-pyrrolo[2,3-d]pyrimidin-4-yl)-2-fluorophenyl]-urea (18t)—52% yield in 4 steps. ¹H-NMR (DMSO-d₆, 400 MHz) δ 12.30 (s, 1H), 8.76 (s, 1H), 7.85 (d, *J* = 9.0 Hz, 3H), 7.80 (d, *J* =

8.6 Hz, 2H), 7.63 – 7.56 (m, 4H), 7.51 (dd, $J = 11.4, 1.8$ Hz, 1H), 7.45 (dd, $J = 8.3, 1.7$ Hz, 1H), 3.91 (t, $J = 6.3$ Hz, 2H), 3.10 (qd, $J = 7.3, 4.8$ Hz, 3H), 2.95 (dd, $J = 11.9, 6.0$ Hz, 2H), 2.37 (s, 3H), 1.92 (d, $J = 4.5$ Hz, 3H), 1.18 (t, $J = 7.3$ Hz, 4H). LC/MS ($M+H^+$): 453.14.

1-(4-Chlorophenyl)-3-(4-(5,6-dimethyl-7H-pyrrolo[2,3-*d*]pyrimidin-4-yl)-2-fluorophenyl)-1-(2-(dimethylamino)ethyl)urea (18w)—54% yield in 4 steps. 1H -NMR (DMSO- d_6 , 400 MHz) δ 12.38 (s, 1H), 9.33 (s, 1H), 8.76 (s, 1H), 7.86 (s, 1H), 7.78 (t, $J = 8.2$ Hz, 1H), 7.66 – 7.57 (m, 2H), 7.57 – 7.42 (m, 3H), 4.02 (t, $J = 6.3$ Hz, 2H), 3.21 (s, 2H), 2.86 (s, 6H), 2.36 (s, 3H), 1.91 (s, 3H). HRMS (ESI-Orbitrap), Calcd for $C_{25}H_{26}ClFN_6O$: 481.1919 [$M+H^+$], Found 481.1909.

1-(4-Chlorophenyl)-3-(4-(5,6-dimethyl-7H-pyrrolo[2,3-*d*]pyrimidin-4-yl)-2-fluorophenyl)-1-(2-methoxyethyl)urea (18x)—50% yield in 4 steps. 1H -NMR (400 MHz, DMSO) δ 12.63 (s, 1H), 8.83 (s, 1H), 8.54 (s, 1H), 7.86 (t, $J = 8.2$ Hz, 1H), 7.68 – 7.29 (m, 6H), 3.94 – 3.84 (m, 4H), 3.66 (s, 3H), 2.39 (s, 3H), 1.93 (s, 3H). LC/MS (ESI-Orbitrap), Found 468.14.

Docking of Limk inhibitors into a crystal structure of Limk1

Inhibitor **18b** was prepared for glide docking using LigPrep (Schrodinger, LLC, NY). The chain A of PDB ID 3S95 was prepared using protein preparation wizard in Maestro V 9.8 (Schrodinger, LLC, NY) by removing water molecules and bound ligand, and adding hydrogen atoms. The docking grid was generated around the original ligand with a box size of $18 \times 18 \times 18 \text{ \AA}^3$. Docking was conducted without any constraint. The top scored docking pose was merged to the protein for energy minimization using Prime (Schrodinger, LLC, NY).

Limk1 biochemical assays and kinase profiling

Biochemical assays for all Limk inhibitors and kinase profiling were carried out in Reaction Biology Corporation and followed the protocols described on its website. Compounds were tested in 10-dose IC_{50} mode with 3-fold series dilution starting at $10 \mu\text{M}$ for IC_{50} measurements. Compounds were tested at $1 \mu\text{M}$ with duplicate experiments in profiling assays. Control compound Staurosporine was tested in 10-dose IC_{50} mode with 3-fold serial dilution starting at $10 \mu\text{M}$. Reactions were carried out at $10 \mu\text{M}$ ATP, $1 \mu\text{M}$ substrate cofilin, and 50 nM Limk1 (final concentrations).

In-Cell Western assay in A7r5 cells

A7r5 (15,000 cells/well) were plated in a clear-bottomed Packard View black 96-well plate in $100 \mu\text{l}$ of 10% FBS DMEM:F12 medium and were allowed to attach overnight. The next day, the cells were serum starved in 1% FBS DMEM medium for 2 hr and then treated with the compounds for 1 hr. Cells were then fixed in 4% paraformaldehyde in PBS for 20 min at room temperature (RT) with no shaking. They were then washed once with 0.1 M glycine to neutralize paraformaldehyde for 5 min. Cells were permeabilized with 0.2% Triton X-100 in PBS for 20 min at RT on orbital shaker after which they were washed once with PBS for 5 min. They were then incubated with Licor Blocking Buffer in PBS (1:1 dilution in PBS) for 1–1.5 h rocking at RT. Cells were incubated with primary antibody p-cofilin Ab (Cell

Signaling # 3311) 1:100 dilution in Licor blocking buffer overnight at 4°C. Next day, they were washed twice with PBS-0.1 % Tween 20 (PBST) washing solution for 5 min each at room temperature on the orbital shaker, followed by one wash with Licor Blocking Buffer containing 0.05% Tween-20 for 5 min on the shaker at RT. The cells were then incubated with secondary antibody goat anti-rabbit IR800 (1:500 dilution) for 1 hr at RT in the dark (covered the plate with foil) in Licor blocking buffer-containing Tween-20. Following this, cells were washed twice with PBST for 5 min each at room temperature and then once with Licor blocking buffer-containing 0.05% Tween-20. The wells were then incubated with ToPro 3 stain (nucleic acid staining), diluted 1:4000 in Licor blocking buffer or Licor blocking buffer with 0.05% Tween-20 for 30 min at room temperature in the dark. Finally the plates were washed twice with PBS and analyzed using the Odyssey LICOR Infrared Scanner.

Cofilin phosphorylation cell assay in PC-3 cell lines

PC3 cells were cultured at a density of 0.5×10^6 cells/mL in 60mm culture dishes in 10% FBS RPMI1640 media. Then, the cells were treated with DMSO and the indicated concentration of Limk inhibitors. After incubating for 24 h, the cells were rinsed with ice-cold PBS twice and collected by spinning down at 4°C in 10,000 rpm for 5 min. Cellular lysates were prepared by suspending cells in SDS sample buffer, 120 mmol/L Tris, 4% SDS, 20% glycerol, 0.1 mg/mL bromophenol blue, and 100 mmol/L DTT (pH 6.8). After brief sonication, the lysates were heated at 95°C for 5 minutes. The cell lysates were separated by 12% SDS-PAGE and transferred to Immobilon-P membranes (Millipore Corp.). Immunostaining was done using antibodies specific for phospho-Cofilin (Cell Signaling, #3313) and β -Actin (GeneScript, #A00702) antibodies and the corresponding second antibodies for whole immunoglobulins from mouse or rabbit (Amersham Biosciences). Immunoreactive proteins were detected by chemoluminescence using the Pierce ECL Western Blotting Substrate (Thermo Scientific). We quantified the actual levels of proteins by using the Multigauge ver 3.0 software (Fujifilm). The gels were stained with Coomassie Brilliant Blue R-250 (0.25%) for 1 hour and then destained (all solutions from Bio-Rad) to check the loading amount of protein samples on the gels.

Cofilin phosphorylation cell assay in CEM-SS T cell lines

CEM-SS T cells (1.0×10^6) were treated with a Limk inhibitor at 10 μ M and 1 μ M separately at 37°C for 4 h. Cells were lysed in NuPAGE LDS Sample Buffer (Invitrogen) followed by sonication. Samples were heated at 90°C for 10 minutes, separated by SDS-PAGE, and then transferred onto nitrocellulose membranes (Invitrogen). The membranes were washed in TBST for 3 minutes and then blocked for 30 minutes at room temperature with Starting Block blocking buffer (Pierce). The blots were incubated with a rabbit anti-phospho cofilin (ser3) antibody (1:500 dilution) (Cell Signaling) diluted in 2.5% milk-TBST and rocked overnight at 4°C. The blots were washed three times for 15 minutes, then incubated with goat anti-rabbit 800cw labeled antibodies (Li-cor Biosciences) (1:5000 diluted in blocking buffer) for 1 h at 4°C. The blots were washed three times for 15 minutes and scanned with Odyssey Infrared Imager (Li-cor Biosciences). The same blots were also stripped and reprobed with antibodies against GAPDH (Abcam) as a loading control.

In vitro invasion assay in PC-3 cells

Transwell chambers coated with GFR Matrigel (BD Biosciences) were used for measurement of cell invasion. The matrigel was solidified at 37°C in a humidified incubator the day before the assay. PC3 cells (1×10^3 cells per well) were grown in serum-free RPMI1640 media in the upper side of the insert. The lower well was filled with RPMI 1640 supplemented with 10% FBS with a Limk inhibitor (1 μ M). PC3 cells were incubated at 37°C in a humidified atmosphere containing 5% CO₂ for 48 h. Then transwell membrane was rinsed three times with PBS, and the cells were fixed in 2.5% EM grade glutaraldehyde for 15 min at room temperature (RT) with no shaking. After removing glutaraldehyde by aspirating, the cells were permeabilized with 0.5% Triton X-100 in PBS for 3 min at RT, and they were rinsed three times with PBS. Then, the cells were stained by Gill's hematoxylin No.1 for 15 min at RT, and they were washed by distilled water for three times. To remove any residual stain, the cells were washed by acid alcohol for 3 minutes and then rinsed by distilled water twice. The cells were exposed with 0.04% NH₄OH until a blue color is observed on the membrane and then rinsed by distilled water twice. The membranes were dried overnight, and the stained cells were visualized under Leica DMI3000B microscope.

In vitro migration assay in PC-3 cells

PC3 cells were cultured to confluence at >90% in 6 well culture dishes in 10% FBS RPMI1640 media the day before the assay. Lines were drawn with a marker on the bottom of the dishes. Using a sterile 1 mL pipet tip, the dishes were scratched three separate wounds through the cells moving perpendicular to the line drawn in the step above. The cells were rinsed with PBS twice very gently and added the RPMI1640 media, and the dishes were taken pictures using phase contrast under Leica DMI3000B microscope. Then, the cells were treated with the indicated concentration of a Limk Inhibitor and incubated for 24 h. The dishes were taken pictures to detect closed wound area as describe above, and the closed wound area was analyzed by ImageJ software (Ver 1.48).

In vitro and in vivo DMPK assays

All in vitro (microsomal stability, CYP-450 inhibition, etc.) and in vivo pharmacokinetics studies were carried in the DMPK Core Facility of Scripps Florida. Detailed procedures for these assays have been described in previous publications (ref. 41–42, 46, 48–50, and 52–55), and were also provided in Supporting Information.

Supplementary Material

Refer to Web version on PubMed Central for supplementary material.

Acknowledgments

This project was supported by NIH grants R21-EY021799 (Y.F and P.L) and 1R01CA140956 (J.L), by the Science and Technology Commission of Shanghai Municipality (P.R. China) Grant 12ZR1431100 (Y.Y), and by the Korea Research Institute of Chemical Technology Scholarship SK-1303 (C.M.P).

References

1. Bernard O, Ganiatsas S, Kannourakis G, Dringen R. Kiz-1, a protein with LIM zinc finger and kinase domains, is expressed mainly in neurons. *Cell Growth Differ.* 1994; 5:1159–1171. [PubMed: 7848918]
2. Stanyon CA, Bernard O. LIM-kinase1. *Int J Biochem Cell Biol.* 1999; 31:389–394. [PubMed: 10224665]
3. Mizuno K, Okana I, Ohashi K, Nunoue K, Kuma K, Miyata T, Nakamura T. Identification of a human cDNA encoding a novel protein kinase with two repeats of the LIM/double Zinc finger motif. *Oncogene.* 1994; 9:1605–1612. [PubMed: 8183554]
4. Osada H, Hasada K, Inazawa J, Uchida K, Ueda R, Takahashi T, Takahashi T. Subcellular localization and protein interaction of the human LIMK2 gene expressing alternative transcripts with tissue-specific regulation. *Biochem Biophys Res Commun.* 1996; 229:582–589. [PubMed: 8954941]
5. Bernard O. Lim kinases, regulators of actin dynamics. *Int J Biochem Cell Biol.* 2007; 39:1071–1076. [PubMed: 17188549]
6. Acevedo K, Moussi N, Li R, Soo P, Bernard O. LIM kinase 2 is widely expressed in all tissues. *J Histochem Cytochem.* 2006; 54:487–501. [PubMed: 16399995]
7. Scott RW, Olson MF. LIM kinases: function, regulation and association with human disease. *J Mol Med (Berl).* 2007; 85:555–568. [PubMed: 17294230]
8. Arber S, Barbayannis FA, Hanser H, Schneider C, Stanyon CA, Bernard O, Caroni P. Regulation of actin dynamics through phosphorylation of cofilin by LIM-kinase. *Nature.* 1998; 393:805–809. [PubMed: 9655397]
9. Edwards DC, Sanders LC, Bokoch GM, Gill BN. Activation of LIM-kinase by Pak1 couples Rac/Cdc42 GTPase signaling to actin cytoskeletal dynamics. *Nat Cell Biol.* 1999; 1:253–259. [PubMed: 10559936]
10. Maekawa M, Ishizaki T, Boku S, Watanabe N, Fujita A, Iwamatsu A, Obinata T, Ohashi K, Mizuno K, Narumiya S. Signaling from Rho to the actin cytoskeleton through protein kinases ROCK and LIM-kinase. *Science.* 1999; 285:895–898. [PubMed: 10436159]
11. Vlachos P, Joseph B. The Cdk inhibitor p57(Kip2) controls LIM-kinase 1 activity and regulates actin cytoskeleton dynamics. *Oncogene.* 2009; 28:4175–4188. [PubMed: 19734939]
12. Thirone AC, Speight P, Zulys M, Rotstein OD, Szaszi K, Pedersen SF, Kapus A. Hyperosmotic stress induces Rho/Rho kinase/LIM kinase-mediated cofilin phosphorylation in tubular cells: key role in the osmotically triggered F-actin response. *Am J Physiol Cell Physiol.* 2009; 296:C463–475. [PubMed: 19109524]
13. Hoogenraad CC, Akhmanova A, Galjart N, De Zeeuw CI. LIMK1 and CLIP-115: linking cytoskeletal defects to Williams syndrome. *Bioessays.* 2004; 26:141–150. [PubMed: 14745832]
14. Piccioli ZD, Littleton JT. Retrograde BMP signaling modulates rapid activity-dependent synaptic growth via presynaptic LIM kinase regulation of cofilin. *J Neurosci.* 2014; 34:4371–4381. [PubMed: 24647957]
15. Heredia L, Helguera P, de Olmos S, kedikian G, Sola Vigo F, LaFerla Fea. Phosphorylation of actin-depolymerizing factor/cofilin by Lim-kinase mediates amyloid beta-induced degeneration: a potential mechanism of neuronal dystrophy in Alzheimer's disease. *J Neurosci.* 2006; 26:6533–6542. [PubMed: 16775141]
16. Honma M, Benitah SA, Watt FM. Role of LIM kinases in normal and psoriatic human epidermis. *Mol Biol Cell.* 2006; 17:1888–1896. [PubMed: 16467374]
17. Bongalon S, Dai YP, Singer CA, Yamboliev IA. PDGF and IL-1beta upregulate cofilin and LIMK2 in canine cultured pulmonary artery smooth muscle cells. *J Vasc Res.* 2004; 41:412–421. [PubMed: 15467300]
18. Dai YP, Bongalon S, Tian H, Parks SD, Mutafova-Yambolieva VN, Yamboliev IA. Upregulation of profilin, cofilin-2 and LIMK2 in cultured pulmonary artery smooth muscle cells and in pulmonary arteries of monocrotaline-treated rats. *Vascul Pharmacol.* 2006; 44:275–282. [PubMed: 16524786]

19. Akagawa H, Tajima A, Sakamoto Y, Krischek B, Yoneyama T, Kasuya H, Onda H, Hori T, Kubota M, Machida T, Saeki N, Hata A, Hashiguchi K, Kimura E, Kim CJ, Yang TK, Lee JY, Kimm K, Inoue I. A haplotype spanning two genes, ELN and LIMK1, decreases their transcripts and confers susceptibility to intracranial aneurysms. *Hum Mol Genet.* 2006; 15:1722–1734. [PubMed: 16611674]
20. Harrison BA, Whitlock NA, Voronkov MV, Almstead ZY, Gu KJ, Mabon R, Gardyan M, Hamman BD, Allen J, Gopinathan S, McKnight B, Crist M, Zhang Y, Liu Y, Courtney LF, Key B, Zhou J, Patel N, Yates PW, Liu Q, Wilson AG, Kimball SD, Crosson CE, Rice DS, Rawlins DB. Novel class of LIM-kinase 2 inhibitors for the treatment of ocular hypertension and associated glaucoma. *J Med Chem.* 2009; 52:6515–6518. [PubMed: 19831390]
21. Xu X, Guo J, Vorster P, Wu Y. Involvement of LIM kinase 1 in actin polarization in human CD4 T cells. *Commun Integr Biol.* 2012; 5:381–383. [PubMed: 23060964]
22. Manetti F. HIV-1 proteins join the family of LIM kinase partners. New roads open up for HIV-1 treatment. *Drug Discov Today.* 2012; 17:81–88. [PubMed: 21872676]
23. Vorster PJ, Guo J, Yoder A, Wang W, Zheng Y, Xu X, Yu D, Spear M, Wu Y. LIM kinase 1 modulates cortical actin and CXCR4 cycling and is activated by HIV-1 to initiate viral infection. *J Biol Chem.* 2011; 286:12554–12564. [PubMed: 21321123]
24. Wen X, Ding L, Wang JJ, Qi M, Hammonds J, Chu H, Chen X, Hunter E, Spearman P. ROCK1 and LIM kinase modulate retrovirus particle release and cell-cell transmission events. *J Virol.* 2014; 88:6906–6921. [PubMed: 24696479]
25. Bagheri-Yarmand R, Mazumdar A, Sahin AA, Kumar R. LIM kinase 1 increases tumor metastasis of human breast cancer cells via regulation of the urokinase-type plasminogen activator system. *Int J Cancer.* 2006; 118:2703–2710. [PubMed: 16381000]
26. Davila M, Frost AR, Grizzle WE, Chakrabarti R. LIM kinase 1 is essential for the invasive growth of prostate epithelial cells: implications in prostate cancer. *J Biol Chem.* 2003; 278:36868–36875. [PubMed: 12821664]
27. Davila M, Jhala D, Ghosh D, Grizzle WE, Chakrabarti R. Expression of LIM kinase 1 is associated with reversible G1/S phase arrest, chromosomal instability and prostate cancer. *Mol Cancer.* 2007; 6:40. [PubMed: 17559677]
28. Manetti F. LIM kinases are attractive targets with many macromolecular partners and only a few small molecule regulators. *Med Res Rev.* 2012; 32:968–998. [PubMed: 22886629]
29. Suyama E, Wadhwa R, Kawasaki H, Yaguchi T, Kaul SC, Nakajima M, Taira K. LIM kinase-2 targeting as a possible anti-metastasis therapy. *J Gene Med.* 2004; 6:357–363. [PubMed: 15026997]
30. Manetti F. Recent findings confirm LIM domain kinases as emerging target candidates for cancer therapy. *Curr Cancer Drug Targets.* 2012; 12:543–560. [PubMed: 22414009]
31. Ohashi K, Sampei K, Nakagawa M, Uchiumi N, Amanuma T, Aiba S, Oikawa M, Mizuno K. Damnacanthal, an effective inhibitor of LIM-kinase, inhibits cell migration and invasion. *Mol Biol Cell.* 2014; 25:828–840. [PubMed: 24478456]
32. Park JB, Agnihotri S, Golbourn B, Bertrand KC, Luck A, Sabha N, Smith CA, Byron S, Zadeh G, Croul S, Berens M, Rutka JT. Transcriptional profiling of GBM invasion genes identifies effective inhibitors of the LIM kinase-Cofilin pathway. *Oncotarget.* 2014
33. Rak R, Kloog Y. Targeting LIM kinase in cancer and neurofibromatosis. *Cell Cycle.* 2014; 13:1360–1361. [PubMed: 24698779]
34. Mashiach-Farkash E, Rak R, Elad-Sfadia G, Haklai R, Carmeli S, Kloog Y, Wolfson HJ. Computer-based identification of a novel LIMK1/2 inhibitor that synergizes with salirasib to destabilize the actin cytoskeleton. *Oncotarget.* 2012; 3:629–639. [PubMed: 22776759]
35. Iyengar S, Hildreth JE, Schwartz DH. Actin-dependent receptor colocalization required for human immunodeficiency virus entry into host cells. *J Virol.* 1998; 72:5251–5255. [PubMed: 9573299]
36. Ross-Macdonald P, de Silva H, Guo Q, Xiao H, Hung CY, Penhallow B, Markwalder J, He L, Attar RM, Lin TA, Seitz S, Tilford C, Wardwell-Swanson J, Jackson D. Identification of a nonkinase target mediating cytotoxicity of novel kinase inhibitors. *Mol Cancer Ther.* 2008; 7:3490–3498. [PubMed: 19001433]

37. He L, Seitz SP, Trainor GL, Tortolani D, Vaccaro W, Poss M, Tarby CM, Tokarski JS, Penhallow B, Hung CY, Attar R, Lin TA. Modulation of cofilin phosphorylation by inhibition of the Lim family kinases. *Bioorg Med Chem Lett*. 2012; 22:5995–5998. [PubMed: 22902653]
38. Sleebs BE, Nikolakopoulos G, Street IP, Falk H, Baell JB. Identification of 5,6-substituted 4-aminothieno[2,3-d]pyrimidines as LIMK1 inhibitors. *Bioorg Med Chem Lett*. 2011; 21:5992–5994. [PubMed: 21852129]
39. Sleebs BE, Ganame D, Levit A, Street IP, Gregg A, Falk H, Baell JB. Development of substituted 7-phenyl-4-aminobenzothieno[3,2-d] pyrimidines as potent LIMK1 inhibitors. *Med Chem Commun*. 2011; 2:982–986.
40. Goodwin NC, Cianchetta G, Burgoon HA, Healy J, Mabon R, Strobel ED, Allen J, Wang S, Hamman BD, Rawlins DB. Discovery of a Type III Inhibitor of LIM Kinase 2 That Binds in a DFG-Out Conformation. *ACS Med Chem Lett*. 2014 dx.doi.org/10.1021/ml500242y.
41. Yin Y, Cameron MD, Lin L, Khan S, Schröter T, Grant W, Pocas J, Chen YT, Schürer S, Pachori A, LoGrasso P, Feng Y. Discovery of Highly Potent and Selective Urea-based ROCK Inhibitors and Their Effects on Intraocular Pressure in Rats. *ACS Med Chem Lett*. 2010; 1:175–179. [PubMed: 24900192]
42. Yin Y, Lin L, Ruiz C, Khan S, Cameron MD, Grant W, Pocas J, Eid N, Park H, Schroter T, Lograsso PV, Feng Y. Synthesis and biological evaluation of urea derivatives as highly potent and selective rho kinase inhibitors. *J Med Chem*. 2013; 56:3568–3581. [PubMed: 23570561]
43. Morita Y, Ishigaki T, Kawamura K, Iseki K. Short and Practical Synthesis of *N,N'*-disubstituted *N*-Aryl-1,2-ethylenediamines by a Decarboxylative Ring-opening Reaction Under Nucleophilic Conditions. *Synthesis*. 2007; 16:2517–2523.
44. Goodacre CJ, Bromidge SM, Clapham D, King FD, Lovell PJ, Allen M, Campbell LP, Holland V, Riley GJ, Starr KR, Trail BK, Wood MD. A series of bisaryl imidazolidin-2-ones has shown to be selective and orally active 5-HT_{2C} receptor antagonists. *Bioorg Med Chem Lett*. 2005; 15:4989–4993. [PubMed: 16168649]
45. Beletskaya IP, Bessmertnykh AG, Guillard R. Halo-substituted Aminobenzenes Prepared by Pd-catalyzed Amination. *Synlett*. 1999; 9:1459–1461.
46. Feng Y, Yin Y, Weiser A, Griffin E, Cameron MD, Lin L, Ruiz C, Schürer SC, Inoue T, Rao PV, Schröter T, LoGrasso P. Discovery of Substituted 4-(Pyrazol-4-yl)-phenylbenzodioxane-2-carboxamides as Potent and Highly Selective Rho Kinase (ROCK-II) Inhibitors. *J Med Chem*. 2008; 51:6642–6645. [PubMed: 18834107]
47. Schröter T, Griffin E, Weiser A, Feng Y, LoGrasso P. Detection of myosin light chain phosphorylation – A cell-based assay for screening Rho-kinase inhibitors. *Biochem Biophys Res Commun*. 2008; 374:356–360. [PubMed: 18638453]
48. Feng Y, Cameron MD, Frackowiak B, Griffin E, Lin L, Ruiz C, Schroter T, LoGrasso P. Structure-activity relationships, and drug metabolism and pharmacokinetic properties for indazole piperazine and indazole piperidine inhibitors of ROCK-II. *Bioorg Med Chem Lett*. 2007; 17:2355–2360. [PubMed: 17368019]
49. Feng Y, Chambers JW, Iqbal S, Koenig M, Park H, Cherry L, Hernandez P, Figuera-Losada M, LoGrasso PV. A small molecule bidentate-binding dual inhibitor probe of the LRRK2 and JNK kinases. *ACS Chem Biol*. 2013; 8:1747–1754. [PubMed: 23751758]
50. Chen YT, Bannister TD, Weiser A, Griffin E, Lin L, Ruiz C, Cameron MD, Schürer S, Duckett D, Schröter T, LoGrasso P, Feng Y. Chroman-3-amides as potent Rho kinase inhibitors. *Bioorg Med Chem Lett*. 2008; 18:6406–6409. [PubMed: 18990570]
51. Ahmed T, Shea K, Masters JR, Jones GE, Wells CM. A PAK4-LIMK1 pathway drives prostate cancer cell migration downstream of HGF. *Cell Signal*. 2008; 20:1320–1328. [PubMed: 18424072]
52. Yin Y, Lin L, Ruiz C, Cameron MD, Pocas J, Wayne G, Schröter T, Chen W, Duckett D, Schürer SC, LoGrasso P, Feng Y. Benzothiazole as Rho-associated Kinase (ROCK-II) Inhibitors. *Bioorg Med Chem Lett*. 2009; 19:6686–6690. [PubMed: 19837589]
53. Fang X, Yin Y, Wang B, Yao L, Chen YT, Schröter T, Weiser A, Pocas J, Wayne G, Cameron MD, Lin L, Ruiz C, Khan S, Schürer SC, Pachori A, LoGrasso P, Feng Y. Tetrahydroisoquinoline

- derivatives as potent and selective Rho kinase Inhibitors. *J Med Chem.* 2010; 53:5727–5737. [PubMed: 20684608]
54. Chowdhury S, Chen YT, Fang X, Grant W, Pocas J, Cameron MD, Ruiz C, Lin L, Park H, Schröter T, Bannister TD, LoGrasso PV, Feng Y. Amino Acid Derived Quinazolines as Rock/PKA Inhibitors. *Bioorg Med Chem Lett.* 2013; 23:1592–1599. [PubMed: 23416002]
55. Zheng K, Iqbal S, Hernandez P, Park H, LoGrasso P, Feng Y. Design and Synthesis of Highly Potent and Isoform Selective JNK3 Inhibitors: SAR Studies on Aminopyrazole Derivatives. *J Med Chem.* 2014 dx.doi.org/10.1021/jm501256y.
56. Zhou P, Zou JW, Tian FF, Shang ZC. Fluorine Bonding; How Does It Work In Protein-Ligand Interactions? *J Chem Inf Model.* 2009; 49:2344–2355. [PubMed: 19788294]
57. Prudent R, Vassal-Stermann E, Nguyen CH, Pillet C, Martinez A, Prunier C, Barette C, Soleilhac E, Filhol O, Beghin A, Valdameri G, Honore S, Aci-Seche S, Grierson D, Antonipillai J, Li R, Di Pietro A, Dumontet C, Braguer D, Florent JC, Knapp S, Bernard O, Lafanechere L. Pharmacological inhibition of LIM kinase stabilizes microtubules and inhibits neoplastic growth. *Cancer Res.* 2012; 72:4429–4439. [PubMed: 22761334]
58. Yoshioka K, Foletta V, Bernard O, Itoh K. A role for LIM kinase in cancer invasion. *Proc Natl Acad Sci USA.* 2003; 100:7247–7252. [PubMed: 12777619]
59. Wu Y, Beddall MH, Marsh JW. Rev-dependent lentiviral expression vector. *Retrovirology.* 2007; 4:12. [PubMed: 17286866]
60. Wu Y, Beddall MH, Marsh JW. Rev-dependent indicator T cell line. *Curr HIV Res.* 2007; 5:394–402. [PubMed: 17627502]
61. Mishima T, Naotsuka M, Horita Y, Sato M, Ohashi K, Mizuno K. LIM-kinase is critical for the mesenchymal-to-amoeboid cell morphological transition in 3D matrices. *Biochem Biophys Res Commun.* 2010; 392:577–581. [PubMed: 20100465]
62. Horita Y, Ohashi K, Mukai M, Inoue M, Mizuno K. Suppression of the invasive capacity of rat ascites hepatoma cells by knockdown of Slingshot or LIM kinase. *J Biol Chem.* 2008; 283:6013–6021. [PubMed: 18171679]
63. Alers JC, Rochat J, Krijtenburg PJ, Hop WC, Kranse R, Rosenberg C, Tanke HJ, Schroder FH, van Dekken H. Identification of genetic markers for prostatic cancer progression. *Lab Invest.* 2000; 80:931–942. [PubMed: 10879743]
64. Yang N, Higuchi O, Ohashi K, Nagata K, Wada A, Kangawa K, Nishida E, Mizuno K. Cofilin phosphorylation by LIM-kinase 1 and its role in Rac-mediated actin reorganization. *Nature.* 1998; 393:809–812. [PubMed: 9655398]
65. Ying H, Biroc SL, Li WW, Alicke B, Xuan JA, Pagila R, Ohashi Y, Okada T, Kamata Y, Dinter H. The Rho kinase inhibitor fasudil inhibits tumor progression in human and rat tumor models. *Mol Cancer Ther.* 2006; 5:2158–2164. [PubMed: 16985048]
66. Hopkins AM, Pineda AA, Winfree LM, Brown GT, Laukoetter MG, Nusrat A. Organized migration of epithelial cells requires control of adhesion and protrusion through Rho kinase effectors. *Am J Physiol Gastrointest Liver Physiol.* 2007; 292:G806–817. [PubMed: 17138966]
67. Nine week old Brown Norway rats (n = 6/group) were housed under constant low light conditions for 65 days (illuminance ranging from 60-80 lux). At 17 weeks, 20 ul of 18w (0.25%) was applied to the right eye. The left eye was untreated and served as the control. IOP measurements were made on both eyes prior to and at 1, 4, 7 and 24 hours post administration. A Tonolab pen was used for IOP measurements. Initial baseline IOP of the treated eye was 28 mmHg. The maximal IOP decrease of the treated eye was ~ 6 mmHg from 1 to 4 hours.

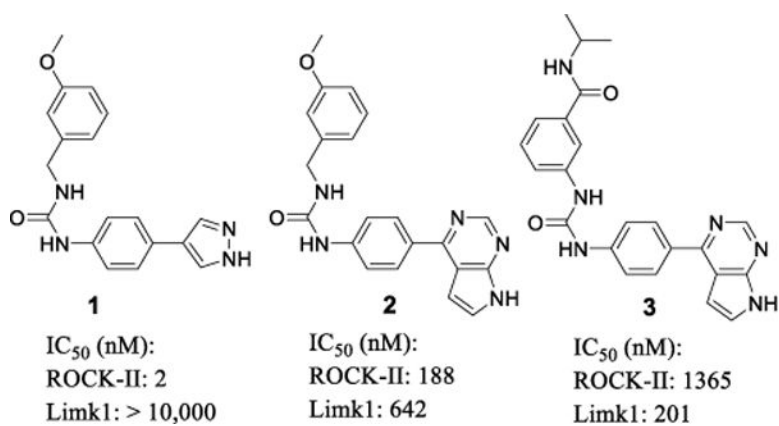


Figure 1. Transition from ROCK inhibition to Limk inhibition for the phenyl urea based scaffold of kinase inhibitors.

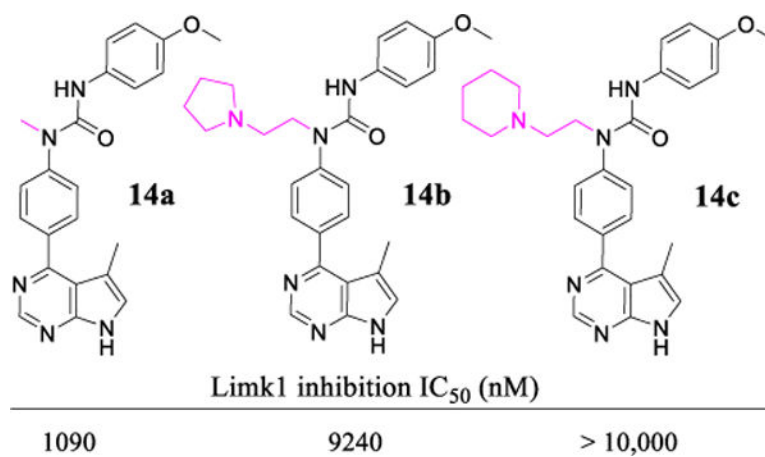


Figure 2.
Substitutions on the urea NH attached to the central phenyl group were not tolerated.

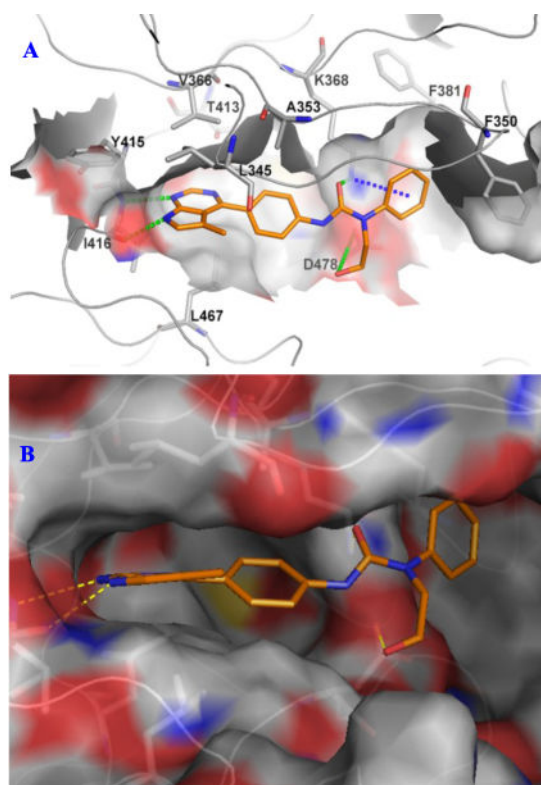


Figure 3. Docking of **18b** to the crystal structure of Limk1 (PDB ID 3S95). A) Schematic view showing key interactions. B) Surface view showing the binding pockets.

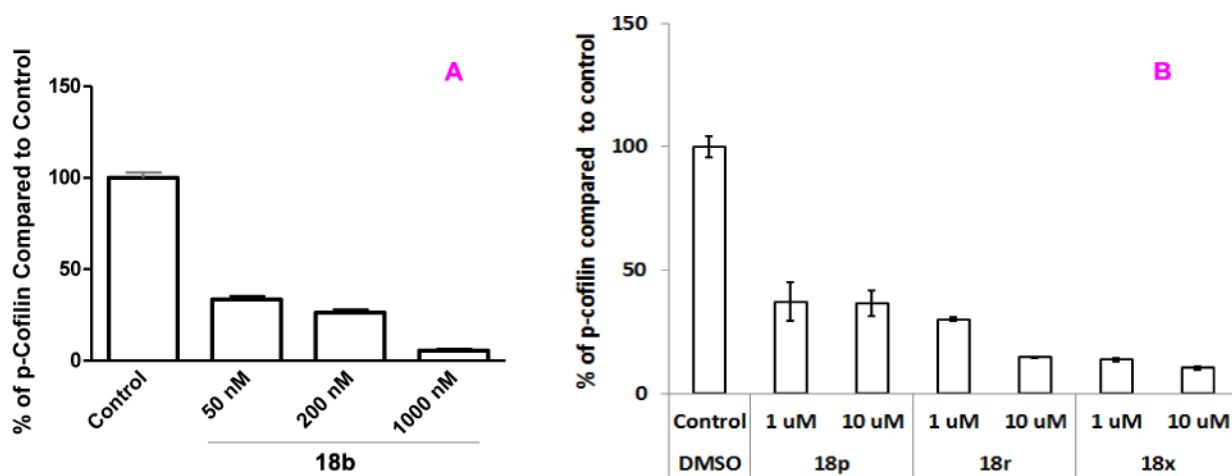


Figure 4.

A: Western blot analysis of p-cofilin in PC-3 prostate cancer cell lines stimulated by HGF treated with **18b**. Similar cell potency was also observed for compound **18f** in PC-3 cells. **B:** Western blot analysis of p-cofilin in CEM-SS T cell lines for **18p**, **18r**, and **18x**.

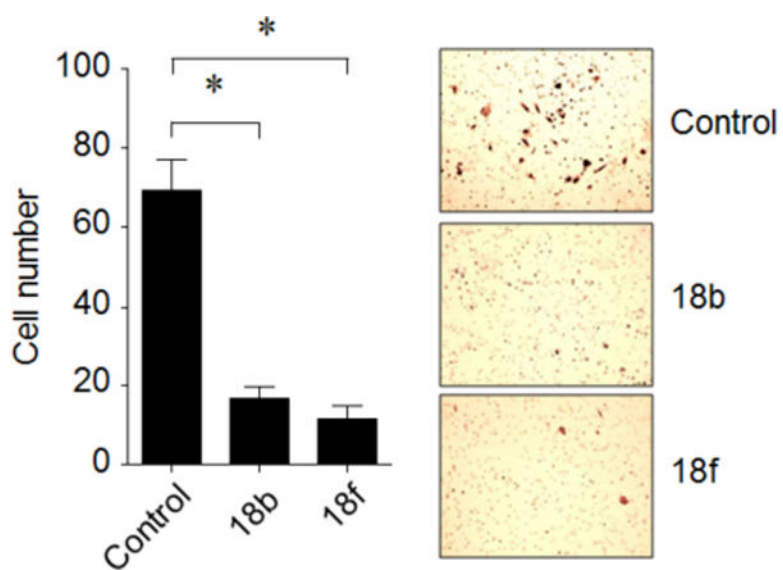


Figure 5. Effect of Limk inhibitors on invasion of PC-3 cell

Comparison of cell invasion (left panel) and phase contrast images (right panel) by treatment of **18b** (1 μ M) or **18f** (1 μ M) for 48 hours in PC-3 cells. The results are shown as mean \pm SD of one representative experiment (from three independent experiments) performed in triplicate. Statically significant differences are indicated (*) $p < 0.05$.

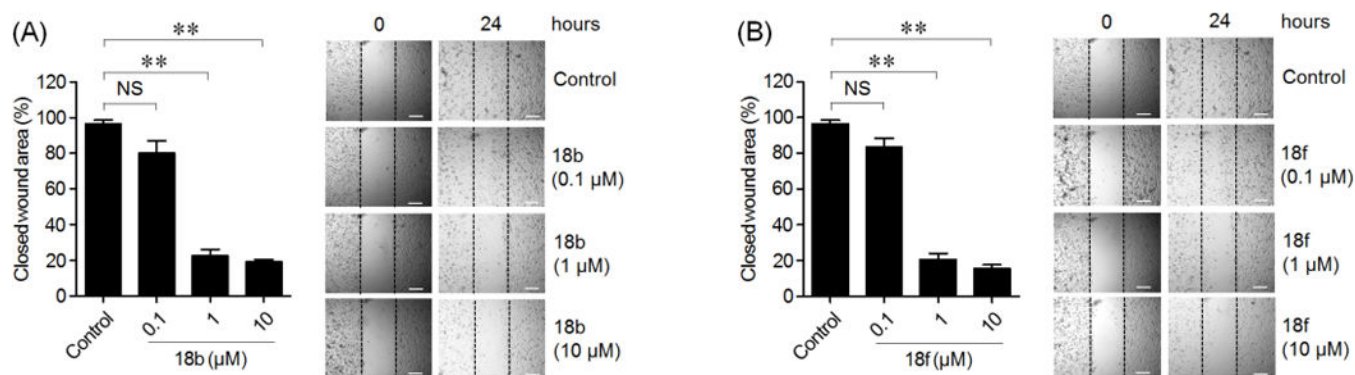


Figure 6. Effect of Limk1 inhibitors on migration of PC-3 cells

Comparison of the average (%) of wound closure (left panel) and phase contrast images (right panel) by treatment with indicated concentration of **18b** (A) or **18f** (B) for 24 hours in PC-3 cells. The results are shown as mean \pm SD of one representative experiment (from three independent experiments) performed in triplicate. Statistically significant differences are indicated (NS) no significance, and (*) $p < 0.01$. Scale bar: 20 μ m.

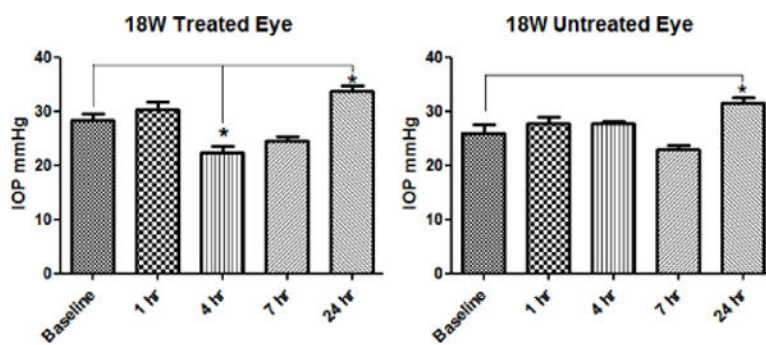
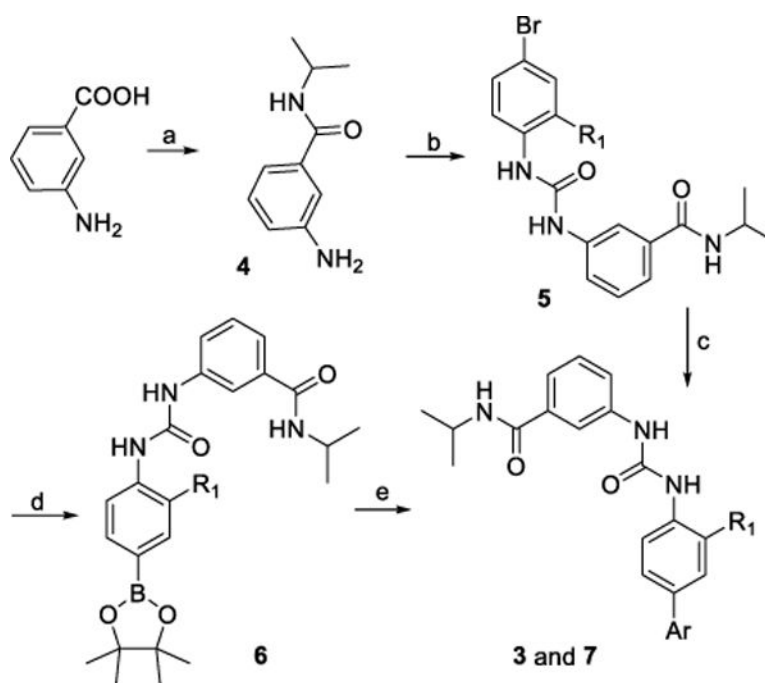


Figure 7. IOP lowering effect of **18w** on rat eyes. Topical dosing at 50 μ g. Data were averaged from 6 determinations (based on 6 rats).

**Scheme 1.**

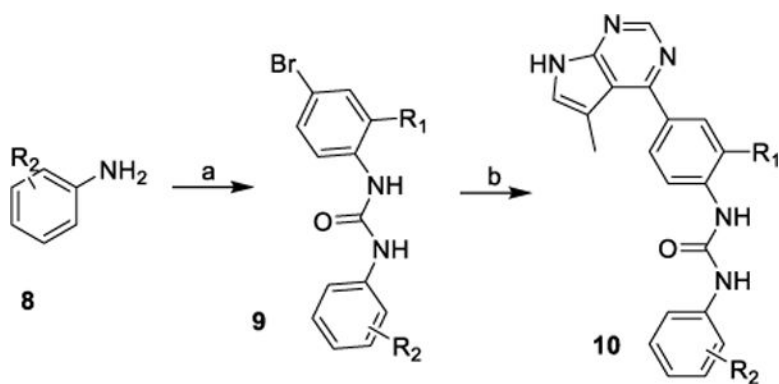
Synthesis of inhibitors 3 and 7.

Reagents and conditions: (a) Propan-2-amine, HATU, DIEA, DMF, rt; (b)

Isocyanatobenzene derivatives, DCM; (c) Boronic acid pinacol ester, Pd(PPh₃)₄,

Dioxane/H₂O, 95 °C; (d) Bis(pinacolato)diboron, PdCl₂dppf, Dioxane, reflux; (e)

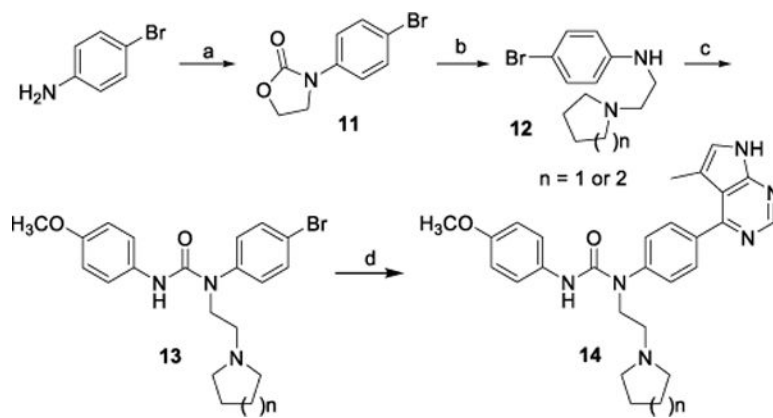
Ar-Cl, Pd(PPh₃)₄, Dioxane/H₂O, 95 °C.

**Scheme 2.**

Synthesis of inhibitor **10**.

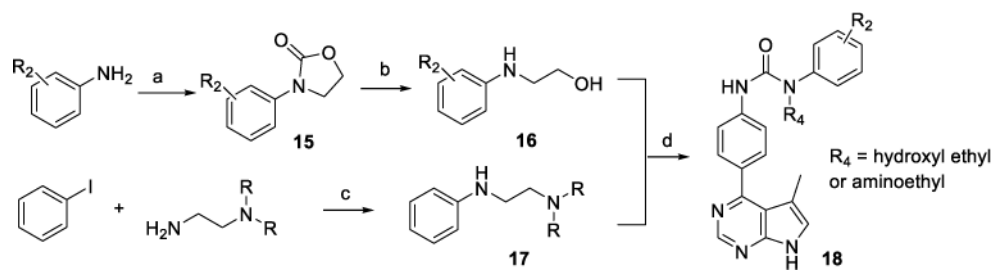
Reagents and conditions: (a) Isocyanatobenzene derivatives, DCM, rt; (b) (i)

Bis(pinacolato)diboron, PdCl₂dppf, Dioxane, reflux; (ii) 4-Chloro-5-methyl-7*H*-pyrrolo[2,3-*d*]pyrimidine, Pd(PPh₃)₄, Dioxane/H₂O, 95 °C.

**Scheme 3.**

Synthesis of inhibitor **14**.

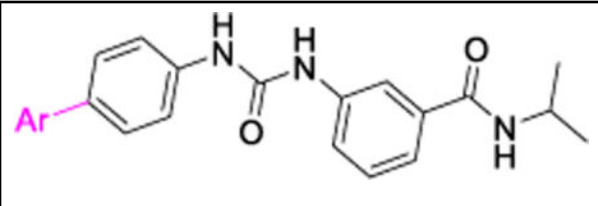
Reagents and conditions: (a) 2-Chloroethyl carbonochloridate, K_2CO_3 , CH_3CN , reflux; (b) Pyrrolidine or piperidine, DMSO, microwave, $110\text{ }^\circ\text{C}$, 1h; (c) 1-Isocyanato-4-methoxybenzene, DCM; (d) (i) *Bis*(pinacolato)diboron, $PdCl_2dppf$, Dioxane, reflux; (ii) 4-Chloro-5-methyl-7*H*-pyrrolo[2,3-*d*]pyrimidine, $Pd(PPh_3)_4$, Dioxane/ H_2O , $95\text{ }^\circ\text{C}$.

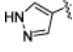
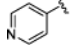
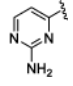
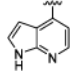
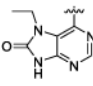
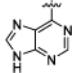
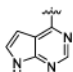
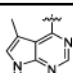
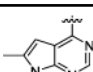
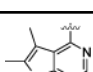
**Scheme 4.**Synthesis of inhibitor **18**.

Reagents and conditions: (a) 2-Chloroethyl carbonochloridate, Py., DCM, rt; (b) KOH, EtOH, reflux; (c) Pd(dba)₂, BINAP, Cs₂CO₃, Dioxane; (d) (i) 1-Bromo-4-isocyanatobenzene, DCM, rt; (ii) Bis(pinacolato)diboron, PdCl₂dppf, Dioxane, reflux; (iii) 4-Chloro-5-methyl-7*H*-pyrrolo[2,3-*d*]pyrimidine, Pd(PPh₃)₄, Dioxane/H₂O, 95 °C.

Table 1

SAR studies of the hinge-binding moiety.

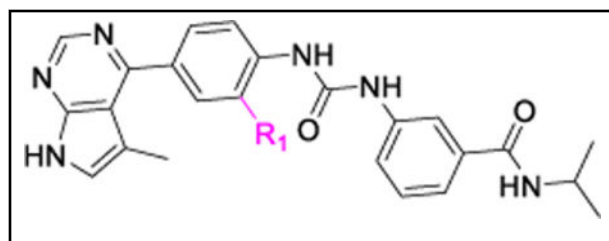


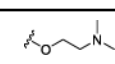
Cmpd	Ar	IC ₅₀ ^a (nM)	
		Limk1	ROCK-II
7a		>10000	45
7b		>10000	90
7c		>10000	166
7d		>10000	132
7e		>10000	247
7f		1527	5570
3		201	1365
7g		62	1608
7h		80	>10000
7i		80	>10000

^aIC₅₀ were means of 2 experiments with errors within 40% of the mean.

Table 2

Effects of substitutions on the central phenyl ring.



Cmpd	R ₁	IC ₅₀ (nM) ^a	
		Limk1	ROCK-II
7g	H	62	1608
7j	CF ₃	60	976
7k	F	18	781
7l		710	7083

^aIC₅₀ were means of 2 experiments with errors within 40% of the mean.

Table 3

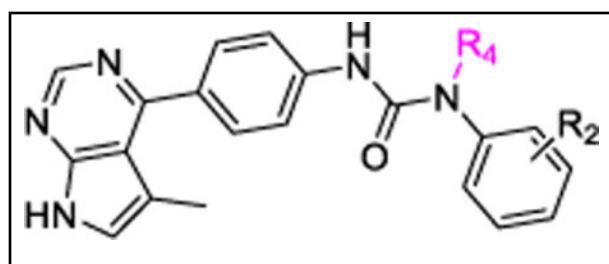
SAR studies on the terminal aromatic ring

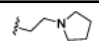
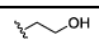
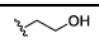
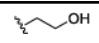
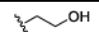
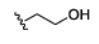
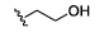
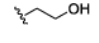
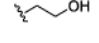
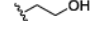
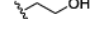
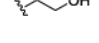
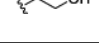

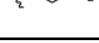
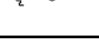
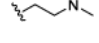
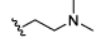
Cmpd	R	IC ₅₀ (nM) ^a	
		Limk1	ROCK-II
10a	H	142	2358
10b	3-F	315	5421
10c	2-OCH ₃	283	6652
10d	3-OCH ₃	75	2572
10e	4-OCH ₃	35	>10,000
10f	–	203	2290
10g	–	4507	>10,000

^aIC₅₀ were means of 2 experiments with errors within 40% of the mean.

Table 4

SAR of the urea NH group attached to the terminal phenyl moiety.



Cmpd	R ₂	R ₄	IC ₅₀ (nM) ^a	
			Limk1	ROCK-II
18a	H		368	nd ^b
18b	H		43	6565
18c	2-F		132	1605
18d	3-F		101	1898
18e	4-F		86	3239
18f	2-Cl		58	3339
18g	3-Cl		67	11270
18h	4-Cl		25	4357
18i	2-CH ₃		350	>10,000
18j	3-CH ₃		151	8940
18k	4-CH ₃		37	5932
18l	2-OCH ₃		913	>10,000
18m	3-OCH ₃		100	3219
18n	4-OCH ₃		53	>10,000
18o	4-OCH ₃		27	nd ^b
18p	4-Cl		21	460
18q	4-OCH ₃		47	>10,000
18r	4-Cl		20	>10,000

^aIC₅₀ were means of 2 experiments with errors within 40% of the mean.

^bNot determined.

Author Manuscript

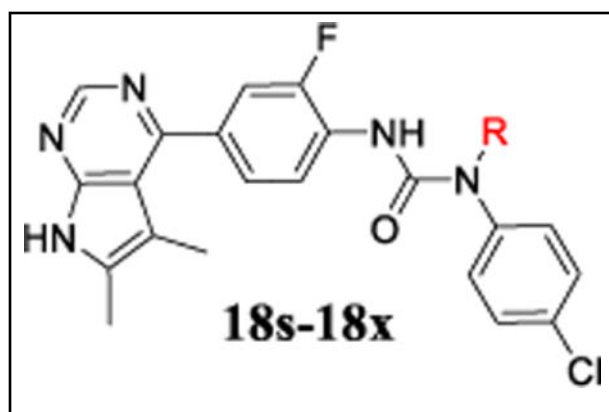
Author Manuscript

Author Manuscript

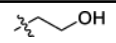
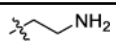
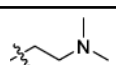
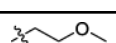
Author Manuscript

Table 5

Biochemical and cell potency for optimized Limk inhibitors.



18s-18x

cmpd	R	Biochemical IC ₅₀ (nM) ^a	
		Limk1	ROCK-II
18s		21	nd ^b
18t		21	nd ^b
18w		19	>20,000
18x		8	>20,000

^aIC₅₀ were means of 2 experiments with errors within 50% of the mean.^bNot determined.

Table 6

Selectivity, microsomal stability, and cell potency data for selected compounds.

Cmpd	Biochemical Inhibition IC ₅₀ (nM) ^a			Microsomal Stability t _{1/2} (min)		Cofilin Phosphorylation In A7r5 Cells (IC ₅₀ , nM) ^a
	ROCK-I	JNK3	P450 % inh. at 10 μM 1A2/C9/2D6/3A4	Human	Rat	
7g	1283	7738	33/49/16/34	33	44	>1000
7i	>20,000	nd ^b	77/42/34/42	47	>120	nd ^b
7k	2390	nd ^b	29/35/13/32	27	55	4000
18b	5536	nd ^b	-16/14/5/13	87	30	470
18e	3920	>10,000	-4/13/3/25	44	52	nd ^b
18f	4390	nd ^b	-4/39/1/37	90	38	420
18g	15,050	nd ^b	-19/31/2/42	22	20	372
18h	5915	> 10,000	-12/23/4/27	>120	73	118
18k	7628	> 10,000	-5/24/-4/5	56	39	190
18m	4317	nd ^b	3/17/3/44	38	21	nd ^b
18n	>20,000	> 10,000	-8/8/-4/2	56	40	730
18s	nd ^b	>10,000	40/13/8/16	99	44	210
18t	nd ^b	>10,000	24/24/52/-11	>120	>120	nd ^b
18w	nd ^b	nd ^b	15/-23/20/-9	19	23	320
18x	nd ^b	>10,000	23/50/15/52	15	13	250

^a IC₅₀ were means of 2 experiments with errors within 40% of the mean.

^b Not determined.

Table 7

Data for Plasma pharmacokinetics studies on rats.^a

Compd	Cl (iv) (mL/min/kg) ^b	V _d (iv) (L/kg) ^b	T _{1/2} (iv) (h) ^b	AUC (iv) (μM* ^h) ^b	C _{max} (iv) (μM) ^b	F (%) ^c (po)
7g	9.0	0.3	1.0	4.3	8.5	0
7k	7.1	0.7	1.5	5.5	5.1	0
10a	3.4	0.5	1.6	14.3	7.0	16
18b	5.2	0.4	2.2	8.4	7.7	36
18f	7.7	0.7	1.5	5.1	4.7	21
18h	3.0	0.5	2.6	13.2	10.5	20
18k	2.7	0.3	1.8	15.6	9.4	24
18n	2.1	0.3	2.2	19.4	10.6	24
18o	36.0	6.0	4.6	1.1	2.2	0
18p	55.9	4.0	5.1	0.7	1.1	0
18r	42.2	17.1	6.1	0.6	0.2	0
18s	4.5	0.5	3.2	14.5	12.3	29
18w	14.2	1.5	3.3	3.0	2.4	nd ^d
18x	6.9	1.2	3.4	5.1	3.5	nd ^d

^aData reported were the mean of three determinations, and the standard error was within 40% of the mean.^biv dosing: 1mg/kg.^cpo dosing: 2 mg/kg.^dNot determined.